JEM Journal of Experimental Medicine

ARTICLE

Disruption of thymic central tolerance by infection with murine roseolovirus induces autoimmune gastritis

Tarin M. Bigley[1], Liping Yang[2], Liang-I Kang[3], Jose B. Saenz[4], Francisco Victorino[2], and Wayne M. Yokoyama[2]

Infections with herpesviruses, including human roseoloviruses, have been proposed to cause autoimmune disease, but defining a causal relationship and mechanism has been difficult due to the ubiquitous nature of infection and development of autoimmunity long after acute infection. Murine roseolovirus (MRV) is highly related to human roseoloviruses. Herein we show that neonatal MRV infection induced autoimmune gastritis (AIG) in adult mice in the absence of ongoing infection. MRV-induced AIG was dependent on replication during the neonatal period and was CD4$^+$ T cell and IL-17 dependent. Moreover, neonatal MRV infection was associated with development of a wide array of autoantibodies in adult mice. Finally, neonatal MRV infection reduced medullary thymic epithelial cell numbers, thymic dendritic cell numbers, and thymic expression of *AIRE* and tissue-restricted antigens, in addition to increasing thymocyte apoptosis at the stage of negative selection. These findings strongly suggest that infection with a roseolovirus early in life results in disruption of central tolerance and development of autoimmune disease.

Introduction

Viruses can induce autoimmune phenomena through a variety of mechanisms (Munz et al., 2009). While molecular mimicry is perhaps the most well-known of these, bystander activation of autoreactive immune cells, epitope spread, and others have also been described (Fujinami and Oldstone, 1985; Munz et al., 2009). These mechanisms are important in humans because, for example, the human roseoloviruses, HHV-6 and HHV-7, have been proposed to be associated with various autoimmune diseases, but how they might trigger autoimmunity remains unknown (Broccolo et al., 2013; Broccolo et al., 2009; Caselli et al., 2017; Caselli et al., 2019; Caselli et al., 2012). Roseoloviruses are ubiquitous β-herpesviruses that infect multiple mammalian species in a species-restricted manner (Denner et al., 2019). Human roseolovirus infections generally present in early childhood as a self-limiting infection characterized by 2–3 d of high fever followed by a transient rash (Agut et al., 2017). After acute infection, roseoloviruses typically become latent, with periodic reactivation, and reach ∼90% prevalence by adulthood (Agut et al., 2017; Cuende et al., 1994). The high prevalence and chronic nature of infections, as well as paucity and limitations of other animal models to date, have confounded establishing a causal relationship between the roseoloviruses and autoimmunity and identifying a potential mechanism (Horvat et al., 2014; Tanner et al., 2013; Wang et al., 2020). These limitations also apply to the association of other viral infections with autoimmunity.

Our lab recently sequenced murine roseolovirus (MRV), demonstrating that it is a murine β-herpesvirus highly related to the human roseoloviruses (Patel et al., 2017). Phenotypically, MRV infection appears to be similar to that of mouse thymic virus (MTV, aka murine herpesvirus 3 or mouse thymic lymphotropic virus), a virus first described in 1961 but that had been lost to study since 1999 (Morse et al., 1999; Patel and Yokoyama, 2017a; Patel et al., 2017; Rowe and Capps, 1961). Both viruses infect the thymus and cause transient CD4 single-positive (SP) and double-positive (DP) thymocyte depletion after neonatal infection (Morse and Valinsky, 1989; Patel et al., 2017). There do appear to be differences between the viruses, as MRV causes thymocyte depletion in mouse strains that were resistant to MTV (Cross et al., 1979; Patel and Yokoyama, 2017a; Rowe and Capps, 1961). Nonetheless, MRV is a natural murine pathogen, providing an opportunity to perform in vivo studies evaluating

[1]Department of Pediatrics, Division of Rheumatology, Washington University School of Medicine, St. Louis, MO; [2]Department of Medicine, Division of Rheumatology, Washington University School of Medicine, St. Louis, MO; [3]Department of Pathology and Immunology, Division of Anatomic and Molecular Pathology, Washington University School of Medicine, St. Louis, MO; [4]Department of Medicine, Division of Gastroenterology, Washington University School of Medicine, St. Louis, MO.

Correspondence to Wayne M. Yokoyama: yokoyama@wustl.edu.

the impact of a viral infection on development of autoimmune disease.

Indeed, a previous study showed neonatal infection with MTV resulted in development of gastric-specific autoantibodies and autoimmune gastritis (AIG) later in life, although disease was limited to BALB/c and A/J mice (Morse et al., 1999). Depletion of $CD4^+$ T cells abrogated gastritis, indicating they play an important pathogenic role in the development of AIG. However, the mechanism responsible for development of AIG after MTV infection was not further studied, particularly with regard to the impact on antigen-presenting cells in the thymus and thymocyte development, which were just beginning to be described (Perniola, 2018). Moreover, the relationship of AIG to viral replication was not explored, since there was no genomic information on MTV, precluding studies determining whether AIG following MTV infection was due to host response to an ongoing, chronic infection. Despite the limitations, the study suggested that an infection with a virus early in life could induce subsequent development of autoimmunity.

AIG has been investigated with respect to T cell tolerance because of the similarities between disease in mice and humans, as well as the known target antigen (D'Elios et al., 2001; Karlsson et al., 1988; Scarff et al., 1997). AIG can be induced in several noninfectious experimental models and is characterized by development of autoreactive $CD4^+$ T cells and autoantibodies that target the hydrogen/potassium (H^+/K^+) ATPase and intrinsic factor on acid-secreting parietal cells, leading to inflammation of the gastric mucosa, specifically within the gastric corpus (Lenti et al., 2020). $CD4^+$ T cells are required for initiating AIG (Sakaguchi et al., 1985; Sakaguchi et al., 1995; Suri-Payer et al., 1999; Suri-Payer et al., 1996). Moreover, $CD4^+$ T cell polarization in the gastric mucosa appears important to the degree of inflammation, with T helper 17 cell (Th17) differentiation being associated with more severe AIG (Bockerstett et al., 2018; Huter et al., 2009; McHugh et al., 2001a; McHugh et al., 2001b; Stummvoll et al., 2008).

Perturbations in central and peripheral tolerance can induce AIG (Barrett et al., 1995; Klocke et al., 2016; Kojima and Prehn, 1981; Perniola, 2018; Winter et al., 2011). Central tolerance occurs in the thymus as T cells undergo affinity-based selection due to recognition of a wide array of self-peptides displayed on thymic antigen-presenting cells, especially medullary thymic epithelial cells (mTECs) and thymic dendritic cells (tDCs; Cheng and Anderson, 2018). DP thymocytes that have not yet developed a TCR capable of interacting with an MHC have low expression of TCRβ and other markers of activation such as CD5, and can undergo death by neglect during positive selection if they fail to form a sufficiently strong MHC–TCR interaction. These cells can be considered to be nonsignaled. Thymocytes with a TCR that do have sufficiently strong interaction with self-MHC are signaled to upregulate TCRβ and CD5 and are then subjected to negative selection, in which clonal deletion occurs due to self-reactive TCRs recognizing self-peptide–MHC complexes with high affinity and/or avidity (Dutz et al., 1995; Hogquist et al., 2005; Ribot et al., 2007). A subset of $CD4^+$ T cells that recognize self-antigen survive and differentiate into regulatory T cells (Tregs) that help mediate peripheral tolerance (Takaba and Takayanagi, 2017).

The autoimmune regulator (AIRE) transcription factor is expressed in mTECs and confers expression of antigens otherwise found in select tissues throughout the body, called tissue-restricted antigens (TRAs; Passos et al., 2018; Takaba and Takayanagi, 2017). H^+/K^+ ATPase consists of an α and β subunit, both of which are expressed in $AIRE^+$ mTECs, although it is unclear how much AIRE influences *ATP4A* or *ATP4B* expression (Bautista et al., 2021; Ruan et al., 2007). Disruption of central tolerance, such as with day 3 thymectomy or in genetic AIRE deficiency, results in development of autoimmunity affecting several organs, including the stomach (Ahonen et al., 1990; Anderson et al., 2002; Kojima and Prehn, 1981; Nishizuka and Sakakura, 1969; Perheentupa, 2006). Development of autoreactive T cells and permanent alterations in Treg populations are seen in both day 3 thymectomy and AIRE deficiency (Asano et al., 1996; Malchow et al., 2016; Sakaguchi et al., 1985; Sakaguchi et al., 1995; Yang et al., 2015). Additionally, disruption of peripheral tolerance by conditional depletion of Tregs results in AIG (Harakal et al., 2016; Sakaguchi et al., 1995). It has therefore been suggested that alterations in both central and peripheral tolerance contribute to development of AIG.

While multiple pathogens have been shown to infect the thymus, induce thymic atrophy or decrease thymocyte number, to our knowledge no previous study has demonstrated a causal link to development of autoimmune disease, such as AIG, especially in the absence of active infection (Savino, 2006; Velardi et al., 2020). Here we found that neonatal MRV infection results in development of AIG and a wide array of autoantibodies. We demonstrate that a thymotropic virus disrupts key components of thymic selection and induces development of autoimmune disease later in life in the absence of ongoing active viral replication.

Results

Neonatal MRV infection results in AIG

Using a modified gastritis scoring system based on inflammatory infiltrate, oxyntic atrophy, and mucous neck cell hyperplasia (Fig. S1 A; Nguyen et al., 2013; Rogers et al., 2005), we found that all BALB/c mice infected with MRV on day of life 0 (D0) developed varying degrees of gastritis (Fig. 1 A). Gastritis was localized to the corpus, as antrum inflammation was not observed (Fig. S1 B). Interestingly, while low levels of MRV DNA were observed at 12 wk postinfection (wpi) by quantitative PCR (qPCR) in the salivary gland, a potential site of chronic infection by MRV and MTV (Cross et al., 1979; Patel and Yokoyama, 2017a), viral DNA was not detectable in the stomach (Fig. 1 B). Thus, these data suggest that gastritis following neonatal MRV infection is not due to local inflammatory responses to ongoing viral replication, but instead may be autoimmune.

AIG due to noninfectious causes is characterized by the development of gastric-specific autoantibodies. Indeed, using immunofluorescence, we observed anti-gastric autoantibodies in sera from BALB/c mice that had been neonatally infected with MRV (Fig. 1 C). The brightest staining was on parietal cells,

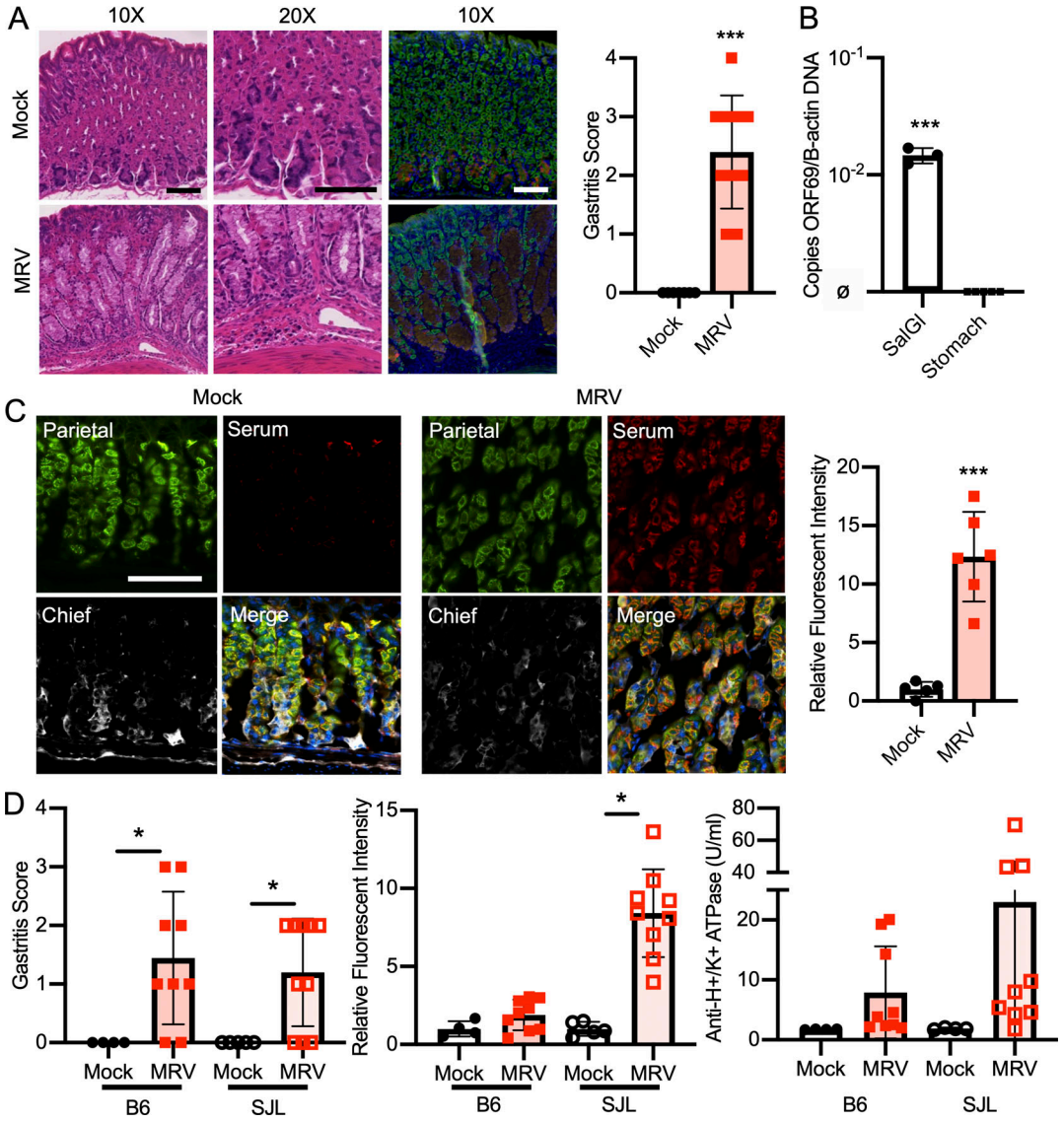

Figure 1. **MRV infection causes AIG and production of autoantibodies. (A)** BALB/c mice were mock-infected (media without virus) or infected with MRV via i.p. injection on D0. Mice were euthanized at 12 wk (mock n = 7, MRV n = 10 from two independent experiments). Stomachs were harvested and prepared for H&E or immunofluorescence staining with DAPI (blue), Ezrin (parietal cells, green), GIF (chief cells, red), or GSII (mucous neck cells, yellow). Images were taken at 10× (scale bar = 100 µm, same scale for all images) or 20× (scale bar = 100 µm, same scale for all images). Blinded gastritis scoring was performed on H&E-stained corpus sections from 12-wk-old BALB/c mice. **(B)** Viral DNA was evaluated from the salivary gland and the stomach (MRV ORF69 copies/B-actin copies; ø indicates no viral DNA detected; mock, n = 3; MRV, n = 5, at least one sample from two separate experiments). **(C)** Stomachs were dissected from uninfected 12-wk-old BALB/c mice and prepared for immunofluorescence. Gastric mucosa was sectioned and stained with 1:10 dilutions of serum from 12-wk-old mice that were mock infected or MRV infected on D0, and representative images are shown: Ezrin (parietal cells, green), serum (red) or GIF (chief cells, white), and Ezrin, serum, and GIF merged with DAPI (blue; Merge). Images were taken at 10× (bar = 100 µM). Relative fluorescence intensity was calculated relative to the average of mock-infected fluorescence. **(D)** C57BL/6 (B6) or SJL/J (SJL) mice were mock or MRV infected via i.p. injection on D0. For C57BL/6: mock, n = 4; MRV, n = 9 (two experiments) and for SJL: mock, n = 5; MRV, n = 10 (two experiments). Mice were euthanized at 12 wk. Stomachs were prepared for H&E, and the corpus was scored for gastritis. Anti-H^+/K^+ ATPase antibody levels were evaluated using fluorescence intensity or anti-parietal cell H^+/K^+ ATPase ELISA. For all gastritis scoring, statistical significance was determined using nonparametric Mann–Whitney U test. Fluorescence intensity and ELISA statistical significance was determined by Student's t test; *, $P < 0.05$; ***, $P < 0.001$.

although faint staining was seen on chief cells as well (Fig. 1 C). Although previous studies with MTV indicated that C57BL/6 mice and several other inbred strains did not develop gastritis (Morse et al., 1999), here we found neonatal MRV infection–induced gastritis in C57BL/6 (7/9 mice) and SJL (7/10 mice; Fig. 1 D). Interestingly, C57BL/6 mice produced less autoantibody than BALB/c and SJL mice, as measured by immunofluorescence intensity as well as ELISA for anti-H^+/K^+ ATPase autoantibodies (Figs. 1 D, 3 D, and S2 F). When we compared development of gastritis and anti-parietal cell autoantibody, we did not observe differences in frequency or degree between male and female mice (Fig. S1 C). Thus, MRV induced AIG with characteristic histological features and parietal cell–specific autoantibody production.

Neonatal MRV infection results in development of a broad repertoire of autoantibodies

While all mouse strains tested were susceptible to developing AIG, we used BALB/c mice in the remainder of this study given the robustness of the phenotype. We next investigated whether neonatal MRV infection resulted in production of autoantibody specificities limited only to gastric antigens. Using an autoantigen microarray, we found a broad repertoire of IgG autoantibodies present in serum of 12-wk-old mice that had been neonatally infected with MRV (Fig. 2). These autoantibodies were not observed in mock-infected mice. The autoantibodies included anti-intrinsic factor antibodies that are typically associated with AIG, as well as autoantibodies associated with disorders such as various autoimmune endocrinopathies (i.e., thrombopoietin [TPO], thyroglobulin, insulin), rheumatic diseases (i.e., double-stranded DNA [dsDNA], topoisomerase I [Scl-70], Sjögren's syndrome type B [SSB], Smith, myeloperoxidase [MPO], glomerular basement membrane [GBM]), autoimmune hepatitis (liver-kidney microsome [LKM]), and others. Although autoreactive IgM antibodies were increased, they were not as diverse as the IgG autoantibodies (Fig. S2 A). Thus, these data suggest that MRV induced a widespread break in immune tolerance resulting in production of a diverse repertoire of autoantibodies.

MRV-induced AIG is dependent on viral replication during the first week of life

Because gastritis induced by neonatal MTV infection or day 3 thymectomy did not develop if the insult occurred after the first few days of life (Morse et al., 1999; Sakaguchi et al., 1985), we investigated whether such timing affected development of AIG induced by MRV. To determine this, we first tested the antiviral activity of ganciclovir (GCV), a nucleoside analogue that inhibits the viral DNA polymerase and limits replication of other β-herpesviruses, including human roseoloviruses (Agut et al., 2017; Nevins and Dunn, 1992). Whereas neonatal MRV infection resulted in failure to gain weight, $CD4^+$ T cell depletion, and thymic atrophy (Patel and Yokoyama, 2017a; Patel et al., 2017), mice treated with GCV after neonatal infection just for the first 7 d of life did not display these features. Namely, they gained weight normally and did not show significant changes in $CD3^+$ T cells, $CD4^+$ T cells, or $CD4^+Foxp3^+$ Tregs (Fig. 3, A and C; and Fig. S2, B and D). Furthermore, at 7 d postinfection (dpi), GCV-treated mice displayed a nearly three-log decrease in viral DNA levels in the thymus and had only low levels of MRV DNA in the stomach (Figs. 3 B and S2 E). We used expression of the putative late viral gene, *ORF69*, as a proxy of viral replication based on previous data demonstrating that robust expression of late genes in other herpesvirus infections is suggestive of active viral replication (Gruffat et al., 2016). We found that GCV treatment resulted in low to undetectable *ORF69* RNA expression, suggesting decreased MRV replication (Fig. 3 B). We did not detect *ORF69* RNA in the stomach, suggesting that there was no MRV replication in the stomach at 7 dpi (Fig. S2 E). At 12 wpi, we found similar low levels of viral DNA in the salivary gland of vehicle- and GCV-treated mice, which suggests that GCV does not induce an abortive infection (Fig. S2 G). As an additional control, mice were infected on D7, which resulted in an intermediate reduction of $CD3^+$ and $CD4^+$ T cells and Tregs compared with the D0 vehicle- and mock-infected controls (Fig. 3 C). We saw that inoculation with $\leq 1{:}10^5$ dilution of the initial viral stock still resulted in depletion of $CD4^+$ T cells 7 d after neonatal infection, making it unlikely that increased mouse weight from D0 to D7 would account for phenotypic differences (Fig. S2 C). These data demonstrate that GCV effectively inhibits viral replication as well as the associated MRV-induced failure to gain weight and $CD4^+$ T cell reduction.

Treatment of D0-infected mice with GCV only for the first 7 d of life, or infection on D7, resulted in a significant reduction in development of gastritis and gastric autoantibody (Figs. 3 D and S2 F). Additionally, treatment with GCV just for the first 7 d of life also reduced the development of diverse autoantibodies observed in untreated MRV-infected mice (Figs. 2 and S2 A). By contrast, mice neonatally infected with MRV and treated with vehicle control developed AIG and autoantibodies at a high frequency (Figs. 3 D and S2 F). Furthermore, starting at 8 wpi, we treated adult MRV-infected mice with a 4-wk course of valganciclovir (VGCV), an oral antiviral with antiviral activities comparable to GCV (Paya et al., 2004; Santos, 2016). VGCV treatment did not reduce gastritis, supporting the conclusion that replication of MRV in adult mice is not necessary for development of AIG (Fig. S2 H). Taken together, MRV-induced autoimmunity is dependent on replication of the virus during the first week of life, suggesting that neonatal disruption of thymic development by MRV drives autoimmunity.

The inflammatory infiltrate of MRV-induced AIG consists of monocytes, eosinophils, and activated $CD4^+$ T cells that are Th2 and Th17 differentiated

We investigated the inflammatory infiltrate of the gastric mucosa in MRV-induced AIG. Using flow cytometry, we found an increase in T cells, specifically CD44-high, CD62L-low ($CD44^+CD62L^-$) $CD4^+$ and $CD8^+$ T cells, in the gastric mucosa of MRV-infected mice compared with mock-infected controls (Fig. 4 A). This phenotype suggested that the majority of the $CD4^+$ and $CD8^+$ T cells in the gastric mucosa of MRV-induced AIG were activated. Additionally, there were increased numbers of Tregs, neutrophils, monocytes, and eosinophils (Fig. 4, A and B). Although there was a trend toward increased B cells and NK cells, it was not statistically significant (Fig. 4 A). These findings were confirmed by immunofluorescence studies at the sites of inflammation, in which we observed $CD4^+$ T cells, $CD8^+$ T cells, $CD11b^+$ cells, and $SiglecF^+$ eosinophils (Fig. 4 C). Thus, our data reveal that the inflammatory infiltrate in MRV-induced AIG is similar to what has been observed in humans and other mouse models (D'Elios et al., 2001; McHugh et al., 2001a; McHugh et al., 2001b; Stummvoll et al., 2008), and we show that there is an increase in Tregs and eosinophils as well.

Because Th cell differentiation in AIG mouse models varies depending on the model, with more severe disease associated with Th17 differentiation (Bockerstett et al., 2018; Stummvoll et al., 2008; Tu et al., 2012), we further evaluated ex vivo cytokine expression in $CD4^+$ T cells in the gastric mucosa. We found an increase in percentage and number of gastric $CD4^+$

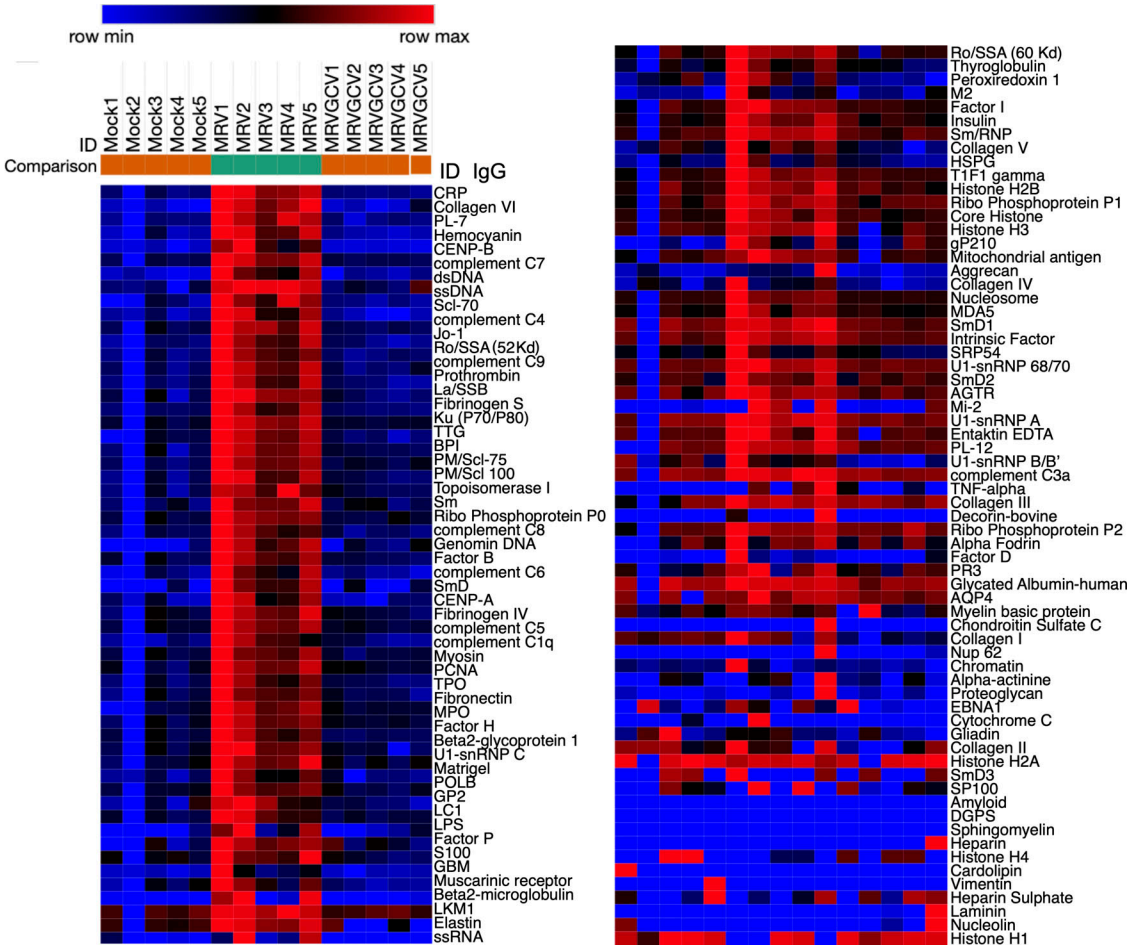

Figure 2. **Neonatal MRV infection results in diverse IgG autoantibody production in adult mice.** BALB/c mice were mock or MRV infected on D0 then treated with vehicle (Veh) control (mock and MRV) or GCV for 7 d (MRV + GCV). At 12 wk, serum was collected (n = 5 individual mice from one experiment) and evaluated using an autoantigen microarray to evaluate levels of IgG autoantibodies, represented as a heatmap. Each column represents serum from one mouse with the indicated experimental condition. The scale represents row minimum and maximum based on the autoantibody levels.

T cells expressing IL-4 or IL-17A in MRV-infected mice by flow cytometry (Fig. 5, A and B). Moreover, immunofluorescence showed IL-17A at the site of inflammation (Figs. 5 C and S2 I). In the spleen, we found that the numbers of activated T cells were similar when comparing mock-infected and D0-infected mice (Fig. S2 J). We then stimulated CD4$^+$ T cells from the spleen and found that, although there was no significant increase in IFN-γ or IL-4 expression in activated CD4$^+$ T cells, there was a small but statistically significant increase in splenic IL-17A$^+$CD44$^+$CD4$^+$ T cells in MRV-infected mice (Fig. S2, J and K). Thus, MRV infection results in a T cell infiltrate in the gastric mucosa consisting of Th2 and Th17 CD4$^+$ cells.

MRV-induced AIG is caused by autoreactive CD4$^+$ T cells

Determining the role of T cells in MRV-induced AIG required careful consideration, because neonatal infection of TCRαβ or CD8 knockout mice results in mortality (Patel and Yokoyama, 2017a). We therefore assessed the necessity of T cells for MRV-induced AIG by using antibody depletion of all αβ-T cells, CD4$^+$ T cells, or CD8$^+$ T cells with specific antibodies given at 6 and 9 wpi (Fig. S3 A), when active infection had subsided (Fig. 7 C) and T cell numbers had recovered (Fig. S4 A). We found that depletion of αβ-T cells and CD4$^+$ T cells significantly decreased development of AIG compared with isotype control, but depletion of CD8$^+$ T cells did not alter gastritis (Fig. 6 A). Given the presence of Th17 cells in the gastric mucosa, we also performed IL-17A blockade with an IL-17A neutralizing antibody given three times weekly for 4 wk and observed significantly reduced development of AIG (Figs. 6 A and S3 D; Faraco et al., 2018; Sell et al., 2015). These data established that CD4$^+$ T cells and IL-17A were necessary for development of AIG.

To evaluate the potential role of B cells, which have an unclear role in other models of AIG (Fukuma et al., 1988; Saito et al., 2016; Suri-Payer et al., 1999), we depleted B cells using an anti-CD20 antibody starting at 6 wk. Depletion of B cells after 6 wk had no significant effect on the histologic evidence of gastritis (Fig. 6 A). On the other hand, neonatal infection of B cell–deficient μMT mice resulted in a reduction of AIG that was not rescued when we transferred serum from 12-wk-old MRV-infected mice (Fig. 6 A). These findings suggest that B cells are necessary for MRV-induced AIG early in life, but B cells and autoantibodies are not the primary mediator of disease after

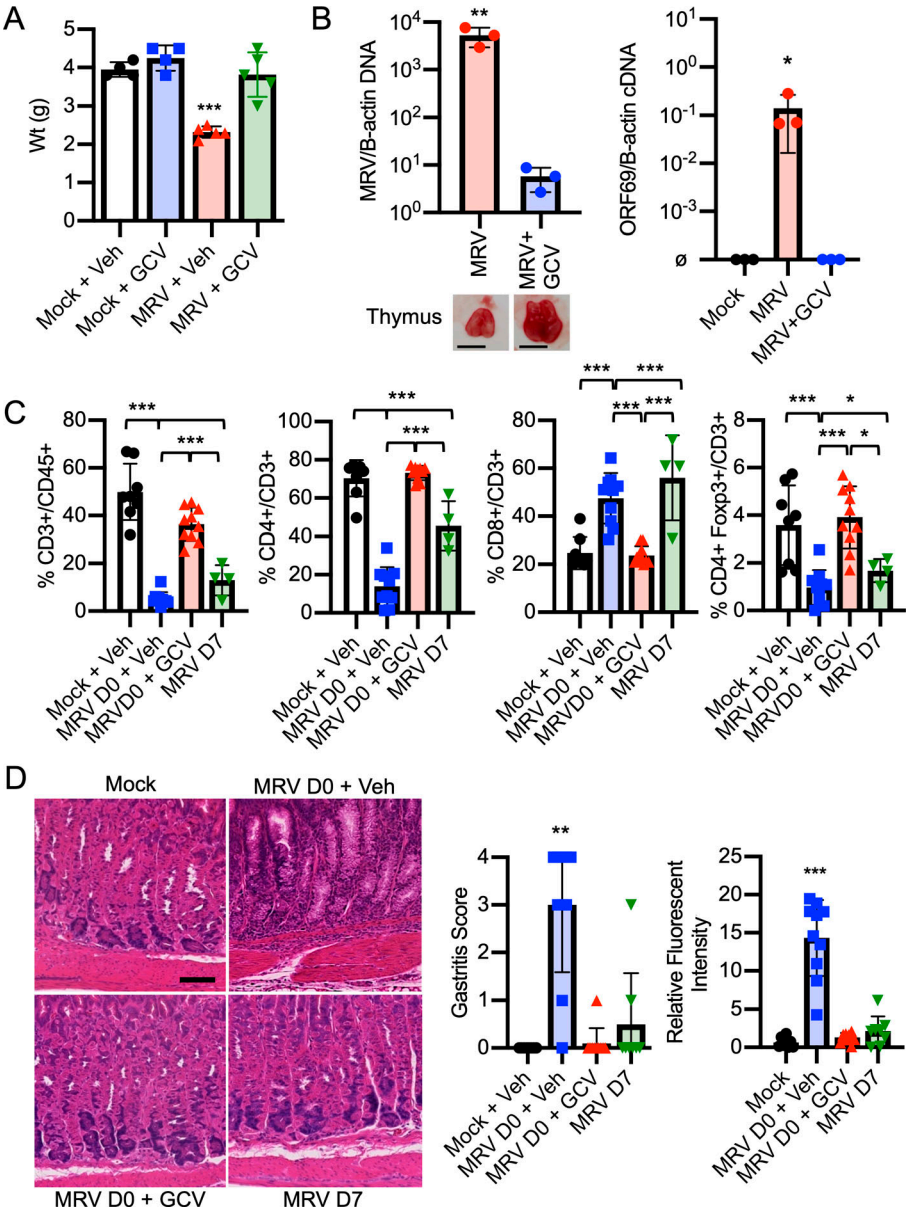

Figure 3. **MRV-mediated AIG is dependent on viral replication before D7.** BALB/c mice were mock or MRV infected on D0 and treated with vehicle control or GCV for 7 d or were infected on D7. **(A)** Mice were weighed on D7 (n = 4 for each condition from one experiment, D7 weights reported from a separate experiment in Fig. S2 D). **(B)** Thymus was harvested on D7 and evaluated for viral DNA (MRV/B-actin), gross thymic size difference (scale bar = 3 mm), or *ORF69* late gene RNA (ORF69/B-actin cDNA, ø indicates below level of detection; n = 3 for each condition from one experiment; Fig. 7 B with additional replicates for cDNA). **(C)** Cheek bleed was performed on D14 and evaluated by flow cytometry (mock, n = 8; MRV D0 + veh, n = 10; MRV D0 + GCV, n = 10; MRV D7, n = 4). **(D)** Gastritis scoring was performed from H&E-stained corpus sections from 12-wk-old mice (mock, n = 8; MRV D0 + veh, n = 10; MRV D0 + GCV, n = 10; MRV D7, n = 8; scale bar = 100 µm, same scale for all images). For C and D, results represent the combined results of two experiments. For A, B (RNA), and C, statistical significance was determined using one-way ANOVA, and Student's t test was used for B (DNA). For gastritis scoring, nonparametric Kruskal–Wallis one-way ANOVA was used. *, P < 0.05; **, P < 0.01; ***, P < 0.001.

6 wk. Of note, we did not observe high levels of MRV DNA in the thymus after depletion of T or B cells, or blockade of IL-17A in adult mice, suggesting that T and B cells and IL-17A are not necessary to control viral reactivation (Fig. S3 E), and that reactivation was not a confounding issue in these studies.

Tregs have previously been demonstrated to reduce autoimmunity in other models of immune dysregulation causing AIG (DiPaolo et al., 2005; Harakal et al., 2016; Suri-Payer et al., 1998; Taguchi and Nishizuka, 1987). More recent work has suggested that neonatal Tregs may have distinct features and increased suppressive capacity compared with adult Tregs (Dong et al., 2017; Mandl et al., 2013; Yang et al., 2015). We therefore isolated either adult (12-wk-old) or neonatal (1-wk-old) CD25$^+$ Tregs from uninfected mice and transferred them to MRV-infected mice 8 wpi. We observed that adoptive transfer of Tregs from adult or neonatal mice resulted in decreased gastritis (Fig. 6 A).

To evaluate which cells were sufficient to induce AIG, we isolated CD4$^+$ T, CD8$^+$ T, and B cells from 12-wk-old mock-infected controls or neonatally MRV-infected mice (Fig. S3, B and C) for transfer to 6–8-wk-old athymic nude mice. Only transfer of CD4$^+$ T cells from neonatally MRV-infected mice resulted in development of gastritis (Fig. 6 B). We then tested whether adult or neonatal Tregs were sufficient to suppress transferred gastritis by isolating conventional CD4$^+$ T cells from MRV-infected mice 12 wpi and cotransferring them with uninfected adult (12-wk-old) or neonatal (1-wk-old) Tregs into 6–8-wk-old athymic nude mice (Fig. S3, B and C). We observed that the majority of mice receiving cotransfer of conventional CD4$^+$ T cells with adult Tregs developed gastritis, while mice receiving the neonatal Treg cotransfer had reduced gastritis compared with those receiving transfer of total CD4$^+$ T cells from MRV-infected mice (Fig. 6 B). Notably, there were no detectable levels of MRV DNA in the salivary glands of mice that received

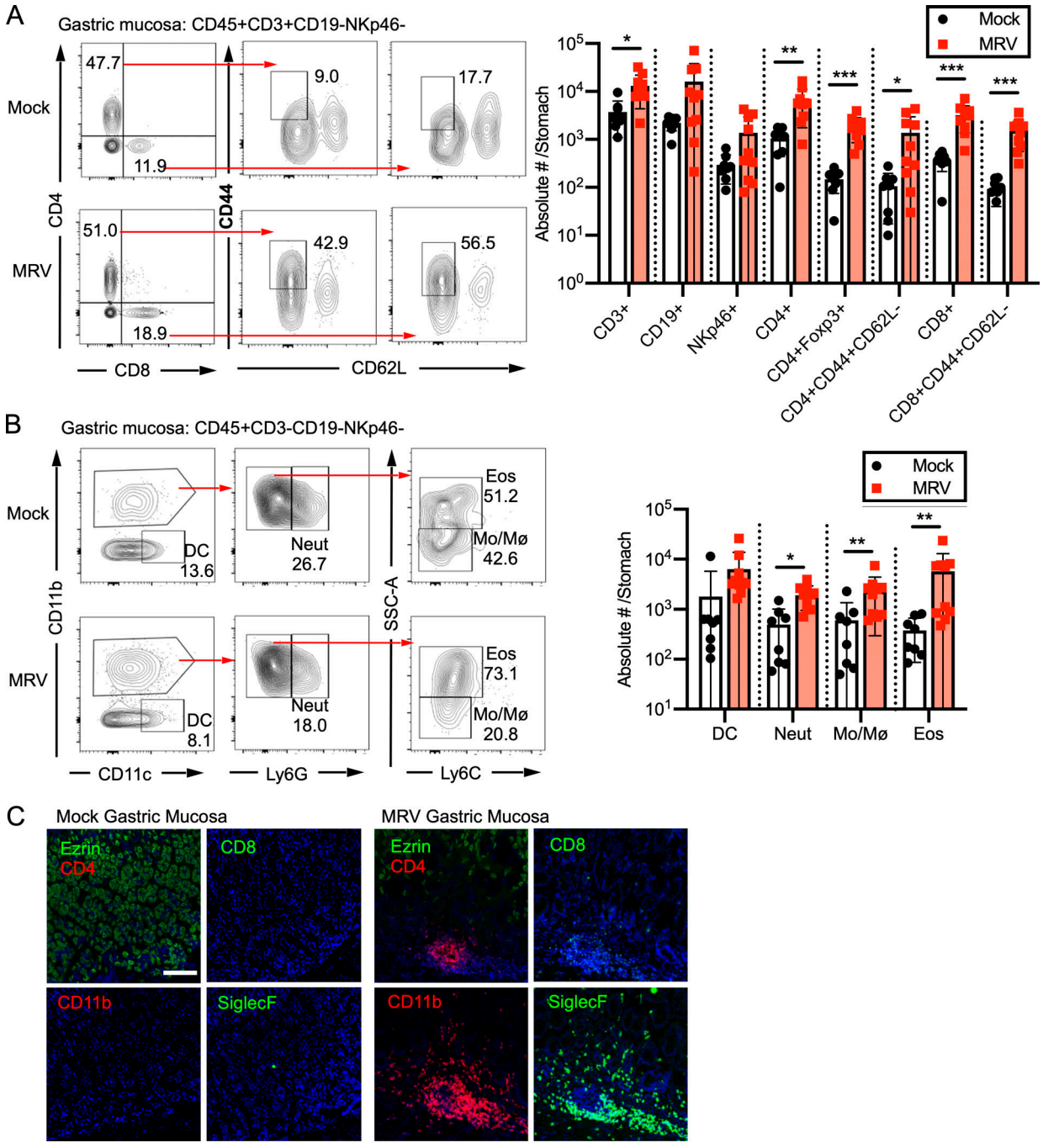

Figure 4. **The inflammatory infiltrate of MRV-mediated AIG comprises T cells, neutrophils, monocytes, and eosinophils.** BALB/c mice were mock or MRV infected on D0. **(A and B)** At 12 wk, stomachs were dissected then digested with collagenase IV to obtain leukocytes. Cells were stained and evaluated by flow cytometry (mock, *n* = 8; MRV, *n* = 10; combined from two independent experiments) for lymphoid populations (A) or myeloid populations (B). Absolute number per stomach was quantified (DC, dendritic cells; Eos, eosinophils; Mo/Mø, monocytes/macrophages; Neut, neutrophils), as indicated in bar graphs. Statistical significance was calculated using multiple Student's *t* test. **(C)** Stomachs were harvested at 12 wk and fixed for immunofluorescence. Representative images of inflammatory foci from three replicates are shown at 10× magnification (scale bar = 100 µm, same scale for all images) with the indicated stain for each panel and DAPI staining in blue. *, P < 0.05; **, P < 0.01; ***, P < 0.001.

adoptive transfer, suggesting that MRV did not reactivate from transferred cells (Fig. S3 G).

We also evaluated the levels of gastric-specific autoantibodies after T and B cell depletion, IL-17A blockade, and Treg adoptive transfer in neonatally infected mice. As in gastritis, we found decreased autoantibody levels after depletion of αβ-T cells and CD4⁺ T cells, as well as blockade of IL-17A (Figs. 6 C and S3 F). Mice that were depleted of CD8⁺ T cells showed similar levels of autoantibodies by immunofluorescence and ELISA compared with isotype control (Figs. 6 C and S3 F). As expected, B cell depletion or deficiency resulted in decreased autoantibody production (Figs. 6 C and S3 F). Despite reducing gastritis,

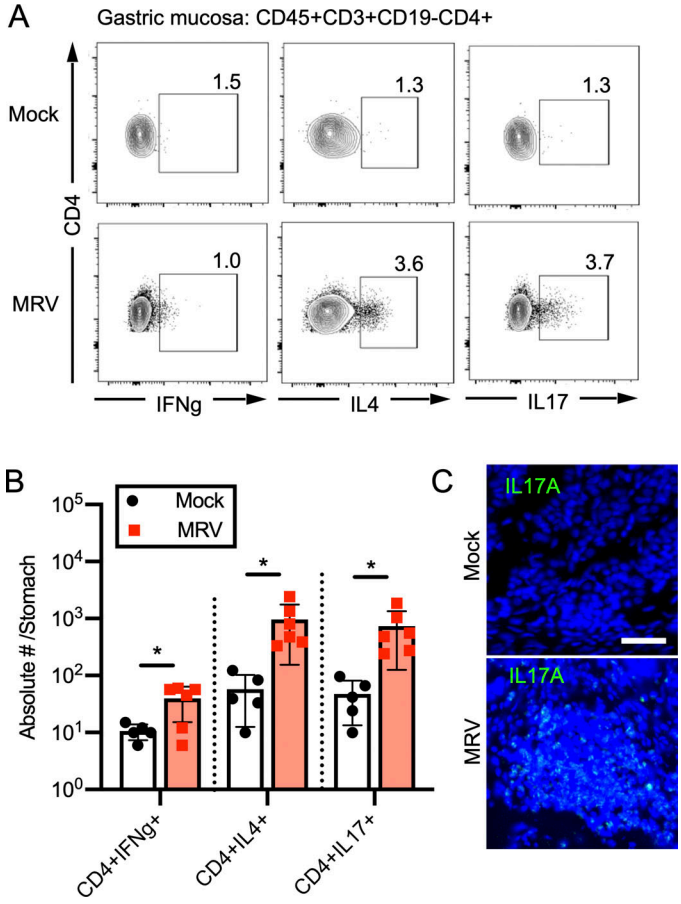

Figure 5. **MRV infection causes Th2 and Th17 skewing in gastric CD4 T cells. (A and B)** Cells were prepared from stomachs as described in Fig. 4, stained ex vivo, and evaluated by flow cytometry for cytokine expression (mock, n = 5; MRV, n = 6 of a representative experiment from two independent experiments; A) which was then quantified as absolute number per stomach (B). Statistical significance was calculated using multiple Student's t test; *, $P < 0.05$. **(C)** Stomachs were harvested at 12 wk and fixed for immunofluorescence. Representative images of inflammatory foci from three replicates are shown for mock and MRV infections (scale bar = 25 µm, same scale for all images).

transfer of adult or neonatal Tregs did not result in a statistically significant reduction in autoantibodies, although there did appear to be a trend toward lower levels (Figs. 6 B and S3 F). There was only low autoantibody production observed in nude mice that had received adoptive transfer of CD4⁺ or CD8⁺ T cells or B cells (Figs. 6 D and S3 H), suggesting that transfer of any of these cells individually was not sufficient to induce autoantibody production. Nonetheless, we have shown that CD4⁺ T cells are necessary and sufficient to cause AIG, demonstrating that neonatal MRV infection induces development of autoreactive CD4⁺ T cells. Furthermore, our data suggest a deficiency in suppressive capacity of the Treg population after neonatal MRV infection that can be rescued by transfer of Tregs from uninfected mice.

Autoantibody production precedes development of MRV-induced gastritis

After neonatal MRV infection, there was a substantial but transient decrease in CD4⁺ T cells in the thymus, as well as a decrease in DP (CD4⁺CD8⁺) thymocytes and peripheral CD4⁺ T cells (Figs. S4 A and S5 A; Patel et al., 2017). CD8⁺ T cell numbers in the thymus were notably less affected by MRV infection (Fig. S4 A), though there was an increase in effector CD8⁺ T cells, as we showed previously (Patel and Yokoyama, 2017a). Interestingly, CD4⁺Foxp3⁺ Tregs showed a significant reduction in numbers at 1, 2, and 4 wpi, with recovery by 8 wpi in the thymus and spleen (Figs. S4 A and S5 A). Previous work in our lab has shown that MRV DNA levels in the thymus peak around D7 after neonatal infection and drop to low levels thereafter (Patel et al., 2017). *ORF69* RNA expression was measured by quantitative RT-PCR (cDNA) as a proxy for MRV replication, which we found peaked around 1 wpi then decreased to nearly undetectable levels by 2 wpi, after which it was no longer detected, suggesting that active viral replication in the thymus does not continue to significant levels after 2 wpi (Fig. 7 C).

Having established the kinetics of CD4⁺ T cell depletion and repletion in the thymus as well as viral replication, we next evaluated how this correlated with development of AIG. At 4 wpi, when CD4⁺ T cell numbers in MRV-infected mice were restored to that of uninfected mice, we did not observe significant gastritis. By 8 wpi, however, inflammatory cell infiltration into the gastric mucosa had begun, although few mice had significant oxyntic atrophy or mucous neck cell hyperplasia (Fig. 7 A). As is observed in some other autoimmune diseases (Arbuckle

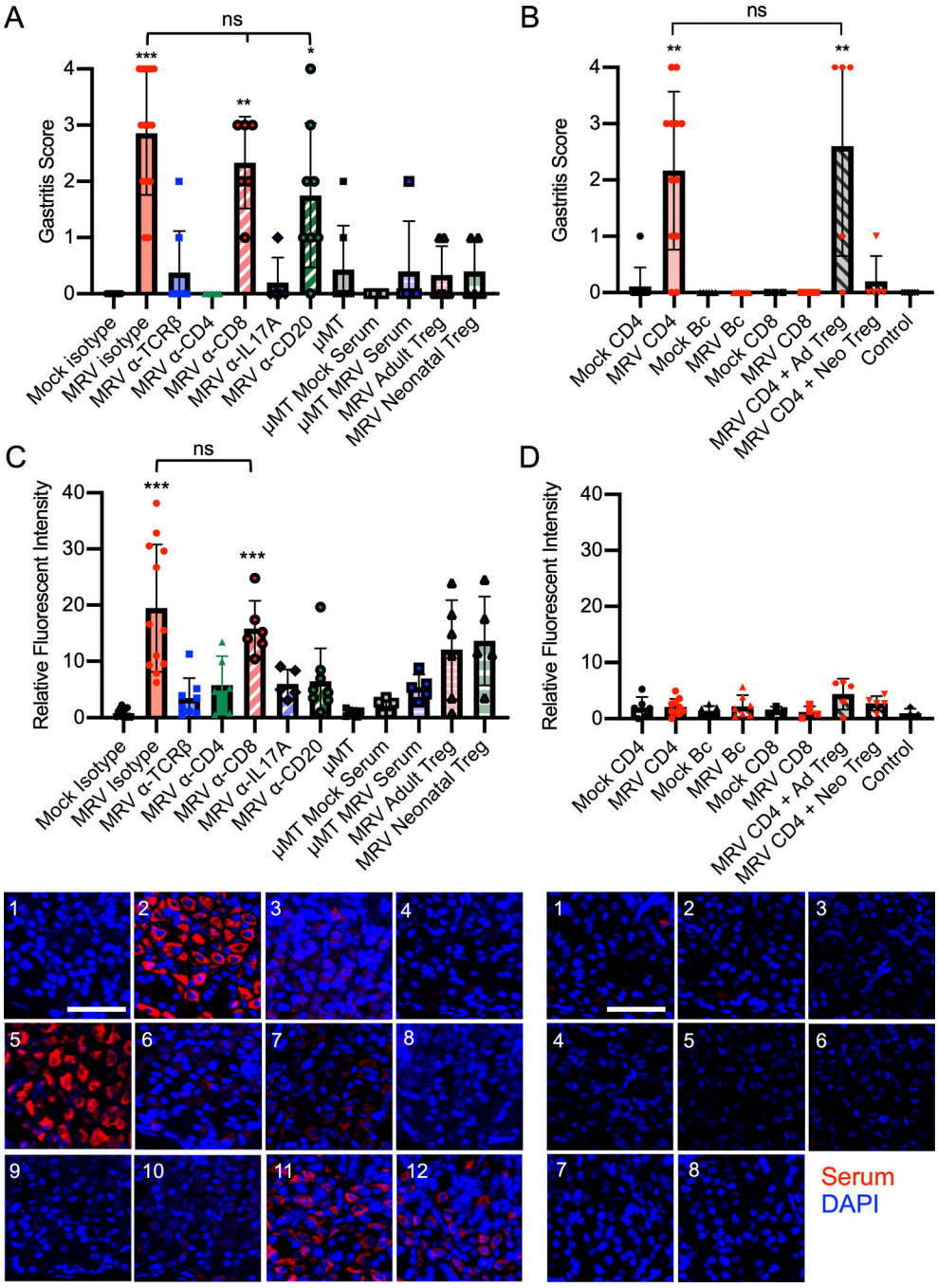

Figure 6. **CD4⁺ T cells are necessary and sufficient for MRV-mediated AIG. (A)** BALB/c or μMT mice were mock or MRV infected on D0. MRV-infected mice were treated with isotype control, anti-TCRβ, anti-CD4, anti-CD8, or anti-CD20 (B cells) starting at 6 wk or anti-IL17A starting at 8 wk. μMT mice were infected with MRV on D0. At 11 wk, μMT mice either remained untreated or were treated with serum from 12-wk-old mock or MRV D0–infected mice. MRV-infected mice received adoptive transfer of 1×10^6 Tregs from uninfected 12-wk-old mice (MRV adult Treg) or 1.5×10^5 uninfected 1-wk-old mice (MRV neonatal Treg) at 8 wpi. At 12 wk, stomachs were harvested, and sections were stained with H&E and evaluated for gastritis score. Results are representative of the combination of two to five separate experiments (mock, $n = 15$; MRV, isotype $n = 14$; MRV anti-TCRβ, $n = 8$; MRV anti-CD4, $n = 6$; MRV anti-CD8, $n = 6$; MRV a-IL17A, $n = 5$; MRV anti-CD20, $n = 8$; μMT, $n = 7$; μMT mock serum, $n = 4$; μMT MRV serum, $n = 5$; MRV adult Treg, $n = 6$; MRV neonatal Treg, $n = 5$). **(B)** BALB/c mice were mock or MRV infected on D0. At 12 wk, splenocytes and lymphocytes from stomach-draining lymph nodes were enriched for CD4⁺ T cells (CD4), B cells (Bc), or CD8⁺ T cells (CD8); alternatively, CD4⁺CD25⁺ T cells (Tregs) were enriched from 12-wk-old adult (Ad) or 1-wk-old neonatal (Neo) mouse spleens and stomach-draining lymph nodes. 1×10^7 enriched CD4⁺, CD8⁺, or B cells were adoptively transferred to 6–8-wk-old athymic nude mice via tail vein injection. For cotransfer, 1×10^7 CD4⁺ conventional T cells from MRV-infected mice were cotransferred with 1×10^6 adult Tregs (MRV CD4⁺ Ad Treg) or with 1.5×10^5 neonatal Tregs (MRV CD4 + Neo Treg). Mice that did not receive adoptive transfer were used as controls. Stomachs were evaluated 6 wk after transfer, fixed, and H&E stained for gastritis scoring from two to three independent experiments (mock CD4, $n = 9$; MRV CD4, $n = 12$; mock Bc, $n = 6$; MRV Bc, $n = 7$; mock CD8, $n = 3$; MRV CD8, $n = 4$; MRV CD4 + Ad Treg, $n = 5$; MRV CD4 + Neo Treg, $n = 5$; control, $n = 7$). **(C)** Stomachs were dissected from uninfected 12-wk-old BALB/c mice and prepared for immunofluorescence. Gastric mucosa was sectioned and stained with 1:10 dilutions of serum collected from mice

described in A and scored for fluorescence intensity relative to mock isotype with representative images shown (1 = mock isotype, 2 = MRV isotype, 3 = MRV anti-TCRβ, 4 = MRV anti-CD4, 5 = MRV anti-CD8, 6 = MRV anti-IL17A, 7 = MRV anti-CD20, 8 = μMT, 9 = μMT mock serum, 10 = μMT MRV serum, 11 = MRV adult Treg, 12 = MRV neonatal Treg). **(D)** Stomachs were harvested from uninfected 12-wk-old BALB/c mice and prepared for immunofluorescence. Gastric mucosa was sectioned and stained with 1:10 dilutions of serum collected from mice described in B and scored for fluorescence intensity relative to mock isotype with representative images shown (1 = mock CD4, 2 = MRV CD4, 3 = mock Bc, 4 = MRV Bc, 5 = mock CD8, 6 = MRV CD8, 7 = MRV + CD4 + Ad Treg, 8 = MRV CD4 + Neo Treg). Nonparametric Kruskal–Wallis one-way ANOVA was used to determine statistical significance of gastritis scoring in A and B. One-way ANOVA was used to calculate statistical significance in C and D. For A and C, asterisks represent statistical difference compared with mock isotype; for B and D, asterisks represent statistical difference compared with control. *, P < 0.05; **, P < 0.01; ***, P < 0.001.

et al., 2003; Leslie et al., 2001; Perniola et al., 2000), we saw that autoantibody production started at 4 wpi and preceded the inflammatory infiltrate and organ damage (Fig. 7, B and D). These findings highlight the kinetics of MRV-induced AIG and autoantibody production, demonstrating that autoantibody production precedes AIG, but that AIG does not develop until weeks after the resolution of CD4⁺ T cell depletion.

Neonatal MRV infection results in depletion of mTECs and tDCs and decreased expression of *AIRE* and TRAs and disrupts thymocyte development

Thus far, we have shown that MRV infection results in a break in CD4⁺ T cell tolerance and alterations in the Treg population that can be rescued by adoptive transfer of Tregs from uninfected mice. Because MRV is thymotropic, we hypothesized that it may impact central tolerance by disrupting mTECs and CD11c⁺ tDCs that normally mediate central tolerance by presenting TRAs to developing T cells for negative selection of autoreactive T cells as well as positive selection of Tregs (Cheng and Anderson, 2018; Passos et al., 2018; Ribot et al., 2007; Zhao et al., 2018). We found that MRV infection on D0 resulted in a reduction in mTECs at 2 and 4 wpi, after which the number of mTECs was similar to mock-infected mice (Figs. 8 A and S4 B), thus demonstrating that mTEC number remain decreased even after CD4 SP and DP thymocyte numbers have recovered (Fig. S4 A). Similar to what we observed in CD4⁺ thymocytes, including CD4⁺Foxp3⁺ T cells (Tregs; Fig. S4 A), CD4⁺ T cells and CD4⁺Foxp3⁺ T cells were significantly reduced in the spleen at 1 and 2 wpi, with a smaller but still significant reduction in conventional CD4⁺ T cells and CD4⁺Foxp3⁺ Tregs at 4 wpi (Fig. S5 A).

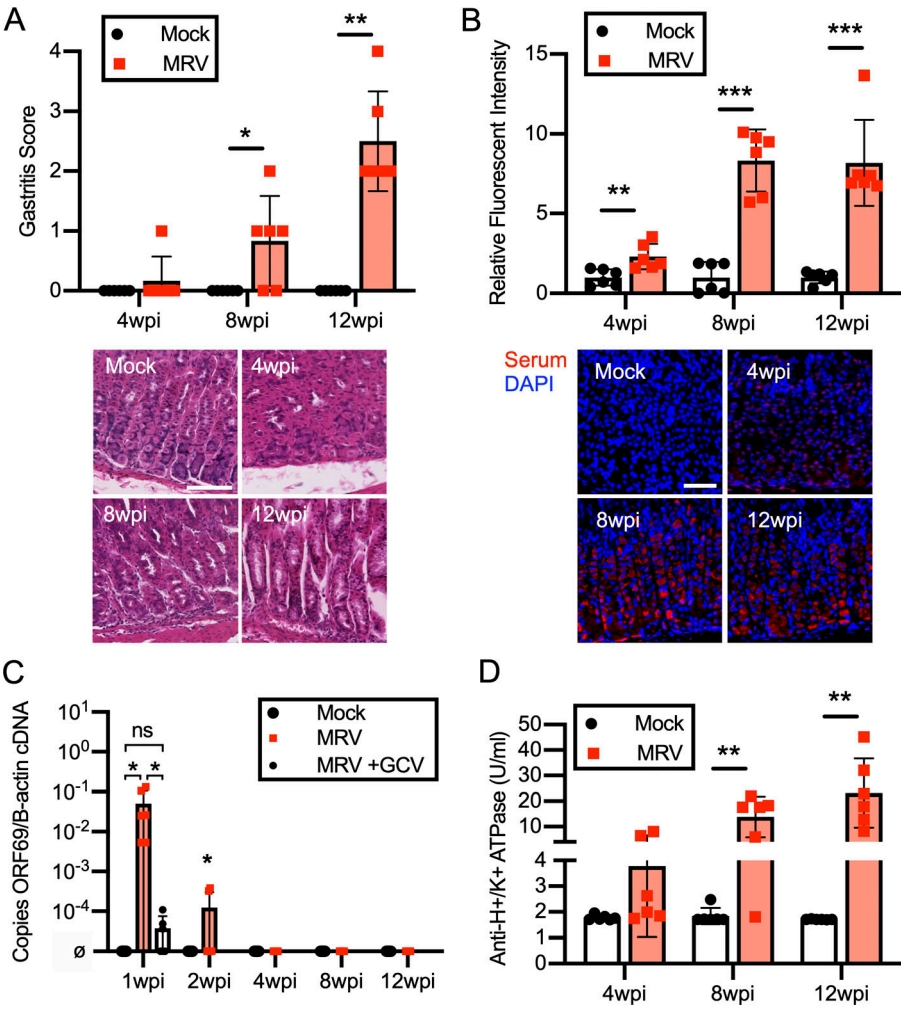

Figure 7. **MRV-induced gastritis is observed after development of autoantibodies.** BALB/c mice were mock or MRV infected on D0 and evaluated at various time points. **(A)** Stomachs were dissected, prepared for H&E staining, and scored for gastritis with representative images shown (scale bar = 100 μm, same scale for all images). **(B)** Stomachs were harvested from uninfected 12-wk-old BALB/c mice and prepared for immunofluorescence. Gastric mucosa was sectioned, stained with 1:10 dilutions of serum, and scored for fluorescence intensity relative to mock infection, with representative images shown (scale bar = 50 μm, same scale for all images; red, serum; blue, DAPI) taken at 40×. **(C)** cDNA prepared from the thymus of D0 mock- or MRV-infected mice was used to perform quantitative PCR (n = 6 from two independent infections; ø indicates below level of detection). **(D)** Anti-H⁺/K⁺ ATPase ELISA was performed on sera collected from mice at 12 wk of life. Statistical analysis for A was performed using multiple comparison nonparametric Mann–Whitney U test. Statistical significance for B–D was determined by multiple comparison Student's t test and one-way ANOVA for 1 wpi in C. *, P < 0.05; **, P < 0.01; ***, P < 0.001.

Interestingly, although the percentage of Foxp3$^+$ cells per CD4$^+$ cells was decreased at 1 and 2 wpi, it was increased at 4 wpi before normalizing, compared with mock at 8 wpi (Fig. S5 B). When we evaluated the number of cortical thymic epithelial cells, which facilitate positive selection, we saw a decrease at 1, 2, and 4 wpi (Fig. S4, A and B). We also observed a transient reduction of tDCs, including CD11c$^+$CD8α$^+$ DCs, at 1 and 2 wpi (Fig. 8 B; and Fig. S4, A and B). These reductions in mTECs and tDCs suggest that MRV disrupts central tolerance early in life.

mTECs express *AIRE*, and deficiency in AIRE results in polyautoimmunity, including polyendocrinopathies and gastritis, in addition to development of multiple autoantibodies (Humbert et al., 2018; Perniola, 2018). We therefore also evaluated expression of *AIRE*. Neonatal MRV infection resulted in decreased *AIRE* expression at 1, 2, and 4 wpi in the thymus (Fig. 8 C), demonstrating that decreased *AIRE* expression continues even after CD4$^+$ thymocyte numbers have normalized (Fig. S4 A). Interestingly, the reduction in *AIRE* expression began before reduction in mTEC numbers, suggesting that MRV infection may impact gene transcription in mTECs. We then assessed expression of TRAs at 7 dpi. Expression of multiple TRAs, such as *ATP4B*, *TPO*, and *Ins2*, was reduced in mice infected with MRV (Fig. 8 D). Inhibition of MRV replication by treatment with GCV rescued expression of *AIRE* and TRAs, further supporting a role for viral replication in loss of tolerance (Fig. 8 D).

Our studies thus far strongly suggest that MRV infection causes a disruption in T cell tolerance in the thymus. To evaluate this further, we considered use of TCR transgenic mice that have been studied extensively in the context of thymic selection (McCaughtry and Hogquist, 2008), but our previous work indicates that T cells, especially CD8$^+$ T cells, are necessary to control infection, limiting the use of TCR transgenics in MRV infection (Patel and Yokoyama, 2017a). We therefore took a flow-cytometry approach in wild-type mice, using expression of CD5 and TCRβ, which is low in nonsignaled thymocytes undergoing positive selection and enhanced in signaled thymocytes undergoing negative selection (Breed et al., 2019). Cleaved caspase 3, which is increased in apoptotic thymocytes during selection, was used to identify nonsignaled cells undergoing death by neglect and signaled cells undergoing clonal deletion. We found that neonatal MRV infection resulted in a decrease in CD5- and TCRβ-high, signaled thymocytes, as well as a significantly increased percentage of signaled thymocytes undergoing apoptosis at the stage of clonal deletion at 5 and 7 dpi (Fig. 8, E and F; and Fig. S5 C). Although there was an increase in the percentage of thymocytes undergoing apoptosis at the stage of death by neglect at 7 dpi, this was less than the percentage and number of cells undergoing apoptosis at the stage of clonal deletion (Fig. 8, E and F; and Fig. S5 C). Interestingly, we did not see a decrease in CD4$^+$ total T cells and Tregs in the thymus or periphery until 5 dpi (Fig. S5, D and E). Together these data suggest that neonatal MRV infection profoundly affects the genes and cells involved in central tolerance and thymocyte development, resulting in autoimmunity.

Discussion

In this study, we demonstrate that AIG develops in adult mice after neonatal infection with MRV. Although the literature suggests that MRV and MTV are related viruses, it has not been definitively demonstrated that they are the same virus, and we provide the first data that MRV can induce AIG and be used to study virus-induced autoimmunity (Patel and Yokoyama, 2017b). Through the use of antivirals and altering the timing of infection, we establish that MRV replication during the neonatal period is necessary for AIG induction. However, AIG occurs at 12 wpi, a time remote to acute infection when we found no evidence of active infection of the stomach. Furthermore, treatment of adult mice with an antiviral did not decrease AIG, indicating that viral reactivation or chronic active infection in adult mice is unlikely to contribute. Finally, we found that MRV induces a large repertoire of autoantibodies, beyond those that are pathogenic in AIG, strongly suggesting that molecular mimicry is unlikely to have caused autoantibody production. Taken together, these data strongly support the conclusion that the autoimmune phenotype is due to broad immune dysregulation related to early MRV infection rather than ongoing, active infection.

Indeed, various infections have been shown to have an effect on the thymus. Among these, one study showed that infection of human thymus with HHV-6A in SCID-hu Thy/Liv mice resulted in thymocyte depletion (Gobbi et al., 1999). Exposure to pathogens early in life can alter the neonatal T cell population (Kidzeru et al., 2014; Marchant et al., 2003; Munks et al., 2006; Rolot et al., 2018). Neonatal infection with murine CMV and adult infection with *Salmonella typhimurium* result in thymic atrophy as well as decreased DP and CD4 SP thymocytes, although neither infection has been reported to result in autoimmunity (Majumdar et al., 2017; Price et al., 1993). Similarly, while *Trypanosoma cruzi*, HIV, measles, lymphocytic choriomeningitis virus, and Zika virus can cause thymic involution and even altered thymic epithelia, a clear link to development of autoimmunity independent of active pathogen replication has not been established (Autran et al., 1996; Elsaesser et al., 2020; Linhares-Lacerda et al., 2015; Messias et al., 2020; Valentin et al., 1999). Moreover, attenuated yellow fever virus was shown to infect the thymus and result in altered expression of *AIRE* and *Foxp3* in the thymus, but there has not been a clear causal link to the development of autoimmunity (Melo-Lima et al., 2015). Thus, while it appears that the thymus is sensitive to alterations after various infections, to our knowledge, our studies are unique in establishing that autoimmune disease can result from a viral infection in the absence of active viral replication in the affected organ.

Our data demonstrate that CD4$^+$ T cells are necessary and sufficient to cause AIG after neonatal MRV infection. This suggests that autoreactive CD4$^+$ T cells are escaping central tolerance, peripheral tolerance, or both. In terms of central tolerance, we found that neonatal MRV infection had significant effects on components of negative selection, including mTEC and tDC numbers as well as expression of *AIRE* and TRAs. Additionally, we demonstrated that MRV disrupted normal thymocyte development during the stage of negative selection, therefore altering the development of conventional and regulatory CD4$^+$ thymocytes early in life. GCV greatly reduced the level of MRV DNA and RNA in the thymus but did not block MRV from getting

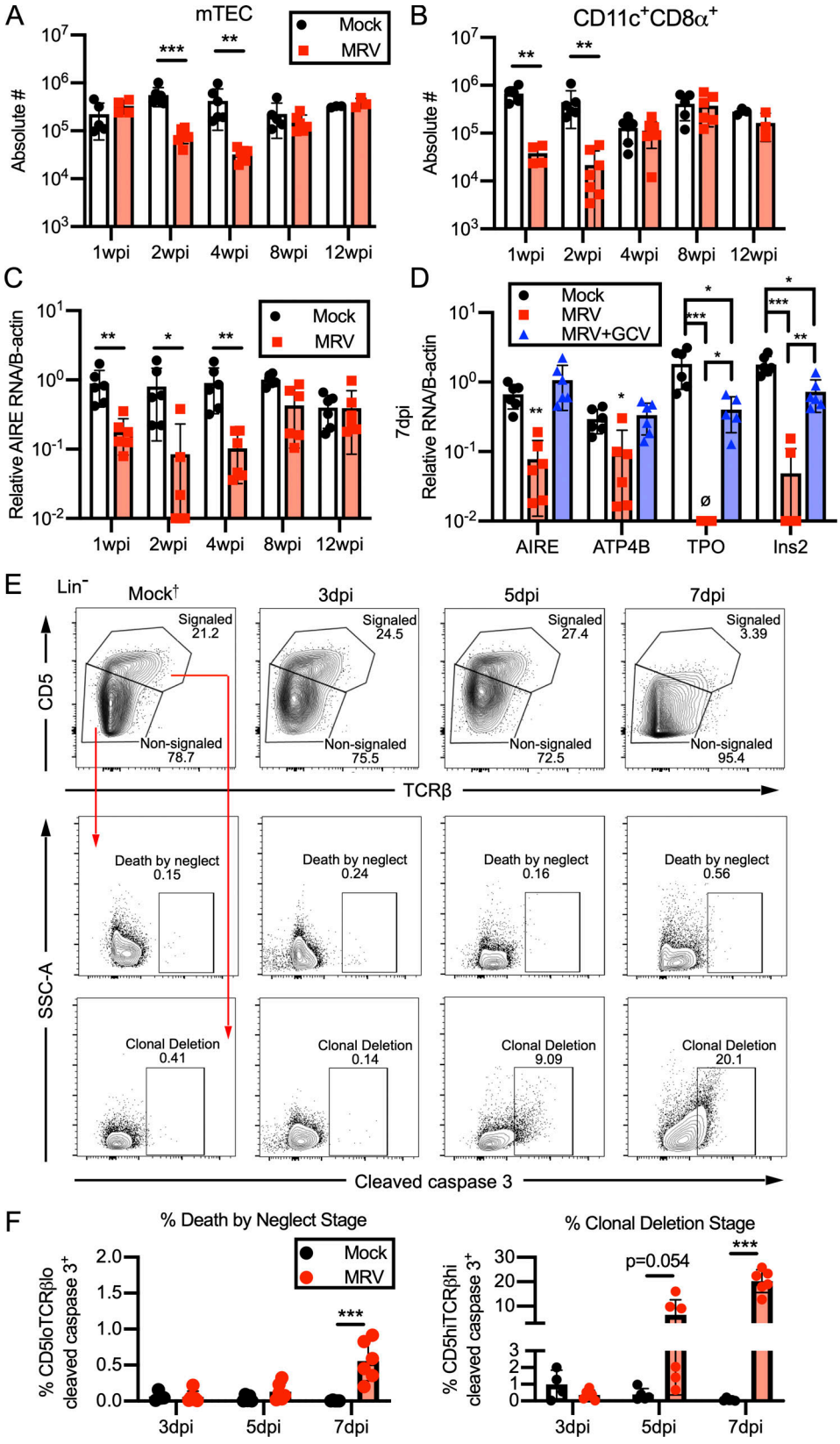

Figure 8. **Neonatal MRV infection results in early reduction in mTECs and tDCs, expression of *AIRE* and TRAs, and increased clonal deletion.** BALB/c mice were mock or MRV infected on D0 and evaluated at various time points. **(A and B)** The thymus was dissected and prepared for flow cytometry to determine absolute cell numbers (#) per thymus for CD45⁻EPCAM⁺UEA-1⁺ mTECs (A) or CD45⁺CD19⁻CD11c⁺ CD8α⁺ (B). **(C and D)** Expression of *AIRE* relative to β-actin (B-actin) in the thymus (C) or AIRE, ATP4B, TPO, and Ins2 relative to B-actin (D) at 7 dpi from mock infection, MRV infection treated with vehicle, or MRV infection treated with GCV. For A–D, data represent two independent infections of n = 3–6 mice for each condition. D0 mock- or MRV-infected thymus

from mice 3, 5, or 7 dpi were evaluated by flow cytometry. **(E and F)** CD19⁻NKp46⁻TCRγδ⁻CD25⁻ (Lin⁻) cells were gated on CD5 and TCRβ surface expression, and cleaved caspase 3–positive cells were gated from signaled ($CD5^{hi}TCR\beta^{hi}$) or nonsignaled ($CD5^{lo}TCR\beta^{lo}$), shown with representative flow plots and percentage of gated cells (E) and percentage of cleaved caspase 3–positive cells per total $CD5^{lo}TCR\beta^{lo}$ (death by neglect stage) or $CD5^{hi}TCR\beta^{hi}$ (clonal deletion stage; $n = 6$ for all except mock 3 dpi [$n = 4$], each from two to three separate infections). Mock†, flow plot is from 7 dpi and representative of mock 3, 5, and 7 dpi. For A–C and F, statistical significance was evaluated using multiple comparison *t* test. For D, statistical analysis for each transcript was evaluated by one-way ANOVA. *, $P < 0.05$; **, $P < 0.01$; ***, $P < 0.001$.

to the thymus and would not inhibit immediate early gene expression, as this antiviral blocks viral replication. Our findings that there were low levels of viral RNA detected in the thymus at 7 dpi and MRV DNA in the salivary gland at 12 wpi in mice treated with GCV for the first 7 days of life suggest that indeed, GCV treatment did not result in abortive infection. Neonatally infected mice treated for the first 7 days of life did not develop AIG, and expression of *AIRE* and TRA was rescued by GCV treatment, providing mechanistic insight into how MRV inhibits central tolerance and induces autoimmunity in a replication-dependent manner. Defining whether MRV infection directly or indirectly causes decreased numbers of thymic antigen-presenting cells and expression changes will require additional tools not yet available for MRV, including an in vitro cell culture system, plaque assays, and virus-specific antibodies. Moreover, roseoloviruses remain latent in host cells and, in the case of HHV-6A and -6B, can integrate into the genome (Pantry and Medveczky, 2017). Although we do not yet know what genes are expressed during latency or whether MRV integrates its genome into the host genome, the ability to study infection in vivo should provide important information about roseolovirus latency and potential impact on autoimmunity.

Autoantibodies were detectable before development of MRV-induced organ-specific autoimmunity. This is similar to many autoimmune diseases in humans, including patients with AIRE deficiency (Ma et al., 2017; Perniola et al., 2000). While MRV infection resulted in reduced but not absent *AIRE* expression, previous studies have suggested that there is a dosage effect of *AIRE* expression and mTECs on T cell development (Garcia-Ceca et al., 2020; Liston et al., 2004). It is therefore interesting to note that whereas thymocyte numbers in our studies normalized by 4 wpi, *AIRE* expression remained decreased compared with uninfected mice. In studies of humans and mice with AIRE deficiency, there are alterations in TCR diversity and Treg development (Hsieh et al., 2006; Malchow et al., 2016; Sng et al., 2019). Furthermore, the autoreactive B cells that develop in AIRE deficiency have been suggested to develop due to loss of peripheral B cell tolerance rather than central B cell tolerance, possibly owing to alterations in T cell–dependent affinity maturation (Kinnunen et al., 2013; Landegren et al., 2019; Ludwig-Portugall et al., 2008; Meyer et al., 2016; Sng et al., 2019; Wardemann et al., 2003; Zhao et al., 2006). The intricacies of how MRV induces autoimmunity remain to be fully determined, but cues from current knowledge of the role of thymic antigen-presenting cells and AIRE functions will be useful for further studies of MRV, human roseoloviruses, and other thymotropic viruses.

In terms of MRV effects on peripheral tolerance, we found that Treg numbers transiently decreased after neonatal infection, but their numbers returned to that of uninfected mice in the thymus and periphery by 8 wpi, when gastritis first started developing. Furthermore, Treg numbers in the gastric mucosa were increased in mice with MRV-induced AIG compared with controls. Although this does not rule out a potential role for Treg alteration in development of AIG, our findings differ from studies of Treg depletion (Harakal et al., 2016) and D3 thymectomy (Yamada et al., 2015), in which AIG began while Treg numbers were reduced, and in the latter case, the Treg population was permanently altered. Despite these Treg findings, our studies revealed that MRV replication during the first week of life is necessary for development of AIG, demonstrating the importance of the timing of infection and raising the possibility that neonatal T cells, including $CD4^+$ conventional and regulatory cells, may also play a role in subsequent autoimmunity. Infection on D7 did result in overall $CD4^+$ T cell depletion, although it was less dramatic than D0 infection. Interestingly, MRV-induced reduction in Treg numbers was similar at 7 dpi after D0 and D7 infection, raising the possibility that alterations in the number of Tregs may be of lesser consequence than the timing of perturbation.

Although T cell differentiation can be impacted by the amount and type of stimulation, as well as developmental age and origin (Cano-Gamez et al., 2020; Jelley-Gibbs et al., 2005; Joshi et al., 2007; Mold et al., 2010; Plumlee et al., 2013; van Faassen et al., 2005; Wang et al., 2016; Zens et al., 2017), neonatal T cells are of particular interest here, especially considering the profound MRV-mediated increase in apoptosis at the stage of clonal deletion starting at 5 dpi. Neonatal T cells develop as the hematopoietic stem cells that populate the thymus undergo a transition from originating in the fetal liver to those originating in the bone marrow around the time of birth (Douagi et al., 2000; Jotereau et al., 1987; Kim et al., 2007). Fetal and neonatal T cells have epigenetic and transcriptional profiles distinct from adult T cells, and they persist into adulthood (Adkins, 2003; Hebel et al., 2014; Rudd, 2020; Yang et al., 2015; Zens et al., 2017; Zhao et al., 2016). Indeed, we found that adoptive transfer of adult or neonatal Tregs to BALB/c mice neonatally infected with MRV did reduce gastritis, although it is important to note that long-lived neonatal Tregs in the adult Treg population would be transferred along with adult Tregs. The neonatal TCR repertoire is more restricted than adult T cells and may be more self-reactive than adult T cells (Dong et al., 2017; Mandl et al., 2013). Interestingly, neonatal Tregs may have more robust suppressive capacity than adult Tregs. This was demonstrated in AIRE-deficient mice, in which neonatal Tregs were able to suppress autoimmunity, while adult Tregs could not (Yang et al., 2015). In concordance with this finding, nude mice that received coadoptive transfer of $CD4^+$ conventional

T cells from neonatally MRV-infected mice with adult Tregs from uninfected mice still developed severe gastritis, while those that received cotransfer with neonatal Tregs had limited to no gastritis. This was despite using 6.7-fold fewer neonatal Tregs than adult Tregs transferred. At this point, it is unclear why transfer of adult Tregs to BALB/c mice reduced disease while cotransfer of adult Tregs with conventional $CD4^+$ T cells to nude mice did not. Several possibilities exist, including the presence of endogenous Tregs and other regulatory cells in BALB/c mice that would not be present in nude mice.

Regarding thymocyte development, we observed increased apoptosis at the stage of clonal deletion after MRV infection, resulting in a considerable decrease in the number and percentage of CD5- and TCRβ-high, signaled thymocytes, likely affecting both Treg and conventional T cell development. Although our previous work suggests that MRV directly infects thymocytes, evidenced by the presence of MRV DNA and viral particles in those cells (Patel and Yokoyama, 2017a), we do not yet know if these cells harbor lytic or latent infection. There are several mechanistic considerations for the apoptosis of signaled thymocytes, including lytic MRV infection of those cells, direct effects of ongoing inflammation, signaling changes from infected stromal cells, or MHC-viral peptide presentation resulting in negative selection of virus-specific thymocytes. The impact of the increased clonal deletion on neonatal Tregs after MRV infection, which has been demonstrated in mice lacking mTECs or functional AIRE, is of considerable interest for MRV-induced autoimmunity (Herbin et al., 2016; Malchow et al., 2016; Perry et al., 2014; Yang et al., 2015). Moreover, further study of the long-term impact of MRV infection on the phenotype of both the neonatal Treg and conventional T cell populations, such as changes in the TCR repertoire, will be necessary to better understand how MRV is altering T cell development and causing loss of tolerance.

Our studies are the first to show that a virus that disrupts thymocyte development can induce development of a wide array of autoantibodies and autoimmune disease later in life after a neonatal infection. While there are scattered reports of neonatal and even congenital infection with human roseoloviruses resulting in lymphopenia, this has not been thoroughly explored, and infection typically occurs later in childhood, between 9 and 21 mo of age (Knox et al., 1995; Lanari et al., 2003; Mendel et al., 1995; Nishizuka and Sakakura, 1969; Yoshikawa et al., 2004; Zerr et al., 2005). We therefore do not yet know how aspects of our studies, such as viral dose, timing of infection, or impact on the immune system, compare to infection with human roseoloviruses, although we now have a system to study these factors. Although viruses have been proposed as a trigger of autoimmune disease, most of those studies have focused on the role of acute or active infection, e.g., HIV- or flavivirus-associated arthritis (Marks and Marks, 2016). Herpesviruses, including HHV-6 and -7, and other chronic infections have been suggested as a possible trigger of autoimmune disease in humans, but their chronic and ubiquitous nature has often made finding a causal link difficult. Moreover, other mechanisms, including molecular mimicry and bystander activation, are generally cited as potential pathogenic possibilities (Munz et al., 2009). Our studies suggest that autoimmunity can occur remote to the acute infection due to alteration in immune development and central tolerance, raising the possibility that viral disruption of the thymus may be a mechanism of autoimmune diseases in humans.

Materials and methods

Mice

BALB/c, C57BL/6, and BALB/c athymic *nu/nu* mice were purchased from Charles River Laboratories. SJL/J mice were purchased from The Jackson Laboratory. In all experiments, mice were bred in-house under specific pathogen–free conditions. MRV-infected and mock-infected mice were housed in separate cages to avoid horizontal transmission. For evaluation of weight, mice were weighed independently. Mouse studies were conducted in accordance with the institutional ethical guidelines through institutional animal care and use committee protocol that was approved by the Animal Studies Committee of Washington University.

Virus stocks and infection

MRV stocks were prepared from in vivo passaging as described previously (Morse et al., 1999; Patel et al., 2017). All experiments shown were performed using a single virus stock, although development of AIG in BALB/c mice was confirmed using an independent virus stock. Briefly, infection of neonatal mice was performed within the first 24 h of life (D0) or on D7 via i.p. inoculation with a 30-gauge needle using 50 µl of a 1:5 dilution of viral stock (2×10^7 viral genomes) in serum-free DMEM. Mock infection was performed by i.p. inoculation with 50 µl of serum-free DMEM. MRV-infected and mock-infected mice were housed in separate cages to prevent horizontal infection, and dams of infected pups were not bred again to avoid potential vertical transmission.

Antiviral treatment

Neonatal mice were treated with 40 µg/g GCV by once-daily i.p. injections (Lenzo et al., 2001). GCV (Thermo Fisher Scientific) was prepared by dissolving powder in sterile water, pH 12, to a concentration of 16 mg/ml, then adjusted to pH 11. Mice were weighed daily for weight-based dose adjustment. Adult mice were treated with VGCV incorporated into chow. VGCV HCl powder (Sigma-Aldrich) was incorporated at 900 ppm, along with red dye, into the standard chow provided in the animal facilities (PicoLab Rodent Diet 20, 5053; LabDiet). Chow was weighed before given. Control mice were given standard chow, and VGCV-treated mice were given a 1:1 diet of regular standard chow mixed with VCGV chow for an estimated dose of 45 µg/g/d. Every 3–4 d, the mice and remaining chow were weighed to ensure equivalent intake of regular and VGCV-containing chow and to calculate dose.

Antibody depletion and neutralization

Depletion and neutralization experiments using primary antibodies were performed via i.p. injection. For depletion of αβ-T cells, 0.5 mg of purified anti-TCRβ antibody (clone H57-597;

Armenian hamster IgG BE0101; BioXCell) was injected on 3 consecutive days in wk 6 and 9 of life. Depletion of $CD4^+$ and $CD8^+$ T cells was performed similarly, with injection on 3 consecutive days in wk 6 and 9 using 0.5 mg of anti-CD4 antibody (clone GK1.5, rat IgG2b; purified in house from hybridoma supernatants) or anti-CD8 antibody (clone 53-6.72, rat IgG2a; purified in house from hybridoma supernatants). Depletion of B cells was performed using 0.25 mg anti-CD20 antibody (clone SA27IG2 Ultra-LEAF; purified rat IgG2b; BioLegend) with a single injection in wk 6 and 9. IL-17A neutralization was performed using 0.5 mg anti-mouse IL-17A antibody (clone 17F3; mouse IgG1; BioXCell) given twice weekly starting in wk 8 (Faraco et al., 2018). For isotype controls of various isotypes, mice were injected as described above using Armenian hamster IgG (purified functional grade; Leinco Technologies), rat hybridoma IgG2b (InVivo; BioXCell), rat hybridoma IgG2a (functional formulation Gold; Leinco Technologies), or mouse IgG1 (BD Biosciences).

Cell enrichment and adoptive transfer

Suspensions of enriched cells for adoptive transfer were prepared from the spleens and stomach-draining lymph nodes of MRV-infected or mock-infected 12-wk-old BALB/c mice. $CD4^+$ T cells, $CD8^+$ T cells, or B cells were enriched using EasySep Cell Separation Kits per manufacturer protocols (Stem Cell Technologies). Cells were counted using a hemocytometer and resuspended in PBS at a concentration of 1×10^7 cells/200 µl except in $CD4^+$ conventional and Treg cotransfer, in which case 1×10^7 conventional $CD4^+$ T cells were combined with 1×10^6 adult Tregs or 1.5×10^5 neonatal Tregs in 200 µl PBS. Cells were kept at 4°C until injection. 1×10^7 cells were injected into the tail vein of each BALB/c athymic *nu/nu* mouse. Enrichment efficiency was evaluated by flow cytometry and was typically >94% (Fig. S3 B). Adoptive transfer was performed in 6–8-wk-old BALB/c *nu/nu* mice that were euthanized for study 6 wk after transfer.

Histopathology, gastritis scoring, and immunofluorescence

Gastric tissue was prepared for histology by washing and inflating stomachs with PBS then fixing in 4% paraformaldehyde (PFA). The forestomach was removed, and stomachs were cut lengthwise into strips that were embedded into paraffin. Slides were prepared by cutting thin sections (5 µm) that were then processed for H&E staining. Images were obtained using a NanoZoomer (Hamamatsu Photonics). Gastritis scoring according to standardized criteria (Fig. S1 A) was assigned independently by two scorers, one a board-certified anatomic pathologist with subspecialty training in gastrointestinal and hepatopancreatobiliary pathology. Both scorers were blinded to the experimental setup. Scores were compared and discussed, with consensus being reached for all samples, which remained blinded to the scorers.

For determination of autoantibodies to gastric mucosal cells, gastric tissue from uninfected mice was prepared as above in 4% PFA followed by paraffin embedding. Tissue sections were mounted on slides, deparaffinized, and incubated in ethanol followed by blocking exogenous peroxide activity with 3% hydrogen peroxide in methanol. Antigen retrieval was performed using 1% antigen masking solution, citrate based (Vector Laboratories). For autoantibody staining, serum that had been collected by terminal exsanguination was diluted 1:10 in blocking buffer (PBS, 3% BSA, 1% saponin, and 1% Triton X-100), or primary antibody was diluted in blocking buffer. Tissue was stained with diluted serum or primary antibodies including anti-Ezrin (3C12; Santa Cruz Biotechnology), anti–gastric intrinsic factor (GIF; kind gift from David Alpers, Washington University, St. Louis, MO), or the lectin GSII Alexa Fluor 594 conjugate (Thermo Fisher Scientific). The secondary antibody, donkey anti-mouse IgG Alexa Fluor 555 or donkey anti-mouse IgG Alexa Fluor 488 (Thermo Fisher Scientific), was diluted 1:1,000 in blocking buffer. Vectashield Hardset Antifade mounting medium with DAPI (Vector Laboratories) was applied to the tissue, and a coverslip was placed. Imaging was performed with a NanoZoomer or on a Nikon Ti Eclipse microscope (Nikon). Quantification of autoantibody and antibody fluorescence intensity was performed using ImageJ v1.51a (National Institutes of Health) of 20× images. Image comparison was performed from images taken with the same exposure and linear adjustment. Fluorescence intensity was calculated using corrected total fluorescence of a 100 × 100-pixel area using: integrated density – [(selected area) × (mean fluorescence of background readings)].

To identify cells in gastric mucosa, histology was performed on gastric tissue by tissue retrieval and processing as described above, followed by fixation in 2% periodate-lysine-PFA fixative at 4°C overnight and incubation in 30% sucrose solution at room temperature for 6 h. Tissue was embedded in optimum cutting temperature medium (Thermo Fisher Scientific) and frozen at −80°C. 9-µm sections were cut and mounted on glass slides. Tissue was stained with anti-Ezrin (3C12; Santa Cruz Biotechnology), anti-CD4 (EPR19514), anti-CD8 (EPR21769), anti-CD11b (EPR1344; Abcam), anti-GIF (kindly provided by Dr. David Alpers, Washington University, St. Louis, MO), or anti-SiglecF (E50-2440; Thermo Fisher Scientific). Secondary antibodies used included donkey anti-mouse IgG Alexa Fluor 555, goat anti-rabbit IgG Alexa Fluor 647, and donkey anti-mouse IgG Alexa Fluor 488 (Thermo Fisher Scientific). Vectashield Hardset Antifade mounting medium with DAPI was added, and images were obtained using the NanoZoomer or Nikon Ti Eclipse microscope.

Flow cytometry

Spleens and stomach-draining lymph nodes were crushed through a 70-µm cell strainer to obtain single-cell suspensions, and red blood cells were lysed using RBC lysis buffer. For analysis of nonstromal thymocytes, the thymus was dissected and minced into fine pieces with scissors. Thymocytes were disrupted from the stroma by pipetting with a large-bore pipette. To analyze thymic stromal cells, the thymus was minced into small pieces with scissors and digested in RPMI containing 0.05% Liberase TL (Sigma-Aldrich) and 100 U/ml DNaseI (Sigma-Aldrich; Jain and Gray, 2014). Cells from the gastric mucosa were obtained by dissection of the stomach followed by thorough washing with PBS and removal of the forestomach. The gastric mucosa was then cut into small pieces, and intraepithelial lymphocytes were removed with HBSS with EDTA,

Hepes, and FCS. EDTA was then washed away, and the tissue was digested with 100 U/ml of collagenase IV (Sigma-Aldrich). The digested sample was passed through a 70-µm filter. To calculate total cells from organs after the above preparations, cells were counted on a hemocytometer.

For stimulation, cells were prepared as described above to achieve single-cell suspensions. 1×10^6 cells were resuspended in RPMI 1640 with 10% FBS, 0.5 µg/ml phorbol myristate acetate (Sigma-Aldrich) and 4 µg/ml ionomycin (Sigma-Aldrich). After 1 h, 1× brefeldin-A (eBioscience) and 5 µg/ml monensin (eBioscience) were added to the medium. Cells were stimulated for 4–5 h, as indicated.

Cells were prepared for flow cytometry by staining with fixable viability dye (eBioscience) and incubated with 2.4G2 hybridoma supernatant to block Fc receptors. Surface staining with fluorescent-labeled antibodies was performed followed by fixation and permeabilization with Foxp3/Transcription Factor Staining Buffer Set (eBioscience). Intracellular staining was performed with Foxp3/Transcription Factor Staining Buffer Set permeabilization buffer. Fluorescent-labeled antibodies used included anti-CD3ε (145-2C11), anti-CD4 (RM4-5), anti-CD8α (53-6.7), anti-Foxp3 (FJK-16 s), anti-CD44 (IM7), Ly6G (1A8), Ly6C (HK1.4), CD5 (53-7.3), and CD11b (M1/70) from Thermo Fisher Scientific; anti-CD19 (6D5), anti-NKp46 (29A1.4), anti-CD62L (MEL-14), anti-EpCAM (G8.8), anti-Ly51 (6C3), anti-CD25 (PC61), anti-TCRγδ (GL3), TCRβ (H57-597), and anti–IFN-γ (XMG1.2) from BioLegend; anti-CD45.2 (104), anti-CD11c (N418), anti–IL-17A (ebio1787), and anti–IL-4 (11B1) from eBioscience; anti–cleaved caspase 3 Asp175 (D3E9) from Cell Signaling; and fluorescent-labeled lectin UEA1 from Sigma-Aldrich. Flow cytometry was performed using a FACSCanto (BD Biosciences) and analyzed using FlowJo v10 (TreeStar).

Analysis of nucleic acids

Nucleic acid analysis was performed from the entire organ except for *AIRE* and TRAs, in which case the thymus was dissected, minced with scissors, and pipetted with a large-bore pipette to remove thymocytes and increase the proportion of stromal cells. DNA was prepared from tissue using Puregene Extraction Kit or QIAAmp Kit (Qiagen), and RNA was prepared from tissue using the RNeasy Plus Kit (Qiagen). cDNA was synthesized from ∼1 µg of DNase-treated RNA reverse transcribed using random hexamers and SuperScript III (Invitrogen). qPCR of DNA and cDNA was quantified using Taqman Universal Master Mix II (Applied Biosystems) on a StepOnePlus real-time PCR machine (Applied Biosystems). For MRV *ORF69* and host *Actb* quantification, a plasmid of known base pair number containing each gene was used to create a standard curve and calculate copies per milliliter. For *AIRE*, *ATP4b*, *TPO*, and *Ins2*, a known quantity of genomic DNA was used to create a standard curve and quantified relative to *Actb* in the sample. Primers used included ORF69 (5′-CAAGTCTGATTGAGGATTCACTTTATG-3′, 5′-56-FAM/TCCAAATCC/ZEN/ACAATTCCCGTCTCTGT/3IABkFQ-3′, and 5′-CGTCGATAGTTGGCAAGAAGA-3′), Actb (5′-AGCTCATTGTAGAAGGTGTGG-3′, 5′-56-FAM/TTCAGGGTC/ZEN/AGGATACCTCTCTTGCT/3IABkFQ-3′, and 5′-GGTGGGAATGGGTCAGAAG-3′), AIRE (5′-GCACACTCATCCTCGTTCT-3′, 5′-56-FAM/TTCCTCCCC/ZEN/TTCCATCCCTCCC/3IABkFQ-3′, and 5′-GGTAGAGATGAGCAGAAAGTGG-3′), ATP4b (5′-CCCGTCCTGCACTTCAATATG-3′, 5′-56-FAM/TAACACTGG/ZEN/TCACCCTGGCATGAC/3IABkFQ-3′, and 5′-ATAGGGACTGTGGTCTCAGAAG-3′), TPO (5′-CTTTTCTAGTTCCTGCCTCTGA-3′, 5′-56-FAM/ACCAAAACC/ZEN/TGTCCCCATCCCTC/3IABkFQ-3′, and 5′-GTCCTCTGTTTGCATGTATCATTG-3′), and Ins2 (5′-AGCGTGGCATTGTAGATCAG-3′, 5′-56-FAM/ATCTGCTCC/ZEN/CTCTACCAGCTGGA/3IABkFQ-3′, and 5′-GTGGGTCTAGTTGCAGTAGTTC-3′).

ELISA and autoantigen array

Serum was collected by terminal exsanguination of anesthetized mice and stored at −20°C. ELISA of anti-parietal (H^+/K^+ ATPase) autoantibody was performed from 1:10 diluted serum using the Parietal Cell ELISA kit (Fitzgerald) per manufacturer's specifications, modified to use HRP-labeled donkey anti-mouse IgG for conjugation (Jackson ImmunoResearch Labs) diluted 1:1,000 in PBS with 0.1% BSA. ELISA of 1:2 diluted serum IL-17A concentrations was performed using the Mouse IL-17A ELISA Kit (Invitrogen) per manufacturer protocol. ELISA plates were read on a BioTek µQuant MQZ200 (BioTek) microplate reader at 450 nm. Autoantigen arrays for IgM and IgG were performed from serum samples by the University of Texas Southwestern Medical Center Microarray Core Facility using the autoantigen microarray super panel. Heatmaps were created using Morpheus open access software (Broad Institute, https://software.broadinstitute.org/morpheus). The heatmap represents relative IgG or IgM autoAb cluster (based on Ab-Score, Abs = $\log_2$ [net fluorescence intensity × signal-to-noise ratio + 1]) as provided by the University of Texas Southwestern Medical Center Microarray Core Facility. The scale of the heatmap represents the Ab-Score relative to row minimum and maximum.

Statistical analysis

The data were analyzed for statistical significance using GraphPad Prism 8. For gastritis scoring, nonparametric Mann–Whitney *U* test was used to compare two groups, and Kruskal–Wallis one-way ANOVA was used to compare more than two groups. For all other analyses, we used Student's *t* test for comparing two samples, multiple Student's *t* test for multiple comparison of two groups, or one-way ANOVA for more than two groups. Statistical significance was denoted as *, $P < 0.05$; **, $P < 0.01$; and ***, $P < 0.001$. Comparisons without significance are not marked except to clarify ns (not significant). Error bars represent SD for all graphs.

Online supplemental material

Fig. S1 shows the gastritis scoring system, with representative images for each score as well as comparison of gastritis and autoantibody levels in male vs. female BALB/c mice. Fig. S2 relates to Fig. 2, showing IgM autoantibody levels from an autoantigen microarray; to Fig. 3, in which MRV stock dilution, D0 MRV infection–induced weight loss, impact of GCV and VGCV on MRV nucleic acid levels, autoantibody levels, and gastritis scores are measured; and to Fig. 5, in which gastric mucosa IL-17A fluorescence intensity and spleen $CD4^+$ T cell cytokine

expression was measured. Fig. S3 displays representative flow cytometry of T and B cells after depletion or enrichment and adoptive transfer, as well as IL-17A levels by ELISA after IL-17A neutralization, MRV DNA levels after depletion, neutralization, μMT infection, or adoptive transfer, and anti-H^+/K^+ autoantibody levels from depletion, neutralization, and adoptive transfer experiments measured by ELISA. Fig. S4 is related to Fig. 8, showing a time course of numbers of various thymus cells after mock versus MRV infection as well as representative flow plots from Fig. 8. In Fig. S5, as in Figs. S4 and 8, a time course is performed demonstrating the number of $CD4^+$ total and Tregs and percentages in the spleen. Fig. S5 also relates to Fig. 8, showing the number of nonsignaled and signaled thymocytes in addition to absolute number of $CD4^+$ populations in the thymus and spleen in mock and MRV D0 infections 3, 5, and 7 dpi.

Acknowledgments

We thank Michael Paley, Anthony French, Jonathan Miner, Chyi Hsieh, Megan Cooper, Sytse Piersma, and the rest of the Yokoyama lab for helpful discussion, guidance, and suggestions on this study. We also appreciate technical advice provided by Nancy Vargas. Finally, we thank David Alpers, who provided the GIF antibody.

This work was supported by funding for T.M. Bigley through National Institutes of Health grants T32AI106688-07 and T32AR007279-40, and a grant from the Barnes-Jewish Hospital Foundation to W.M. Yokoyama.

Author contributions: Conceptualization, T.M. Bigley and W.M. Yokoyama; Methodology, T.M. Bigley, L. Yang, and J.B. Saenz; Investigation, T.M. Bigley, L. Yang, L.-I. Kang, J.B. Saenz, and F. Victorino; Writing—Original and Edited Drafts, T.M. Bigley and W.M. Yokoyama; Writing—Review & Editing, T.M. Bigley, L. Yang, L.-I. Kang, J.B. Saenz, F. Victorino, and W.M. Yokoyama; Resources, T.M. Bigley and W.M. Yokoyama; Supervision, T.M. Bigley and W.M. Yokoyama; Funding Acquisition, T.M. Bigley and W.M. Yokoyama.

Disclosures: The authors declare no competing interests exist.

Submitted: 30 June 2021
Revised: 29 November 2021
Accepted: 24 January 2022

References

Adkins, B. 2003. Peripheral $CD4^+$ lymphocytes derived from fetal versus adult thymic precursors differ phenotypically and functionally. *J. Immunol.* 171:5157–5164. https://doi.org/10.4049/jimmunol.171.10.5157

Agut, H., P. Bonnafous, and A. Gautheret-Dejean. 2017. Update on infections with human herpesviruses 6A, 6B, and 7. *Med. Mal Infect.* 47:83–91. https://doi.org/10.1016/j.medmal.2016.09.004

Ahonen, P., S. Myllarniemi, I. Sipila, and J. Perheentupa. 1990. Clinical variation of autoimmune polyendocrinopathy-candidiasis-ectodermal dystrophy (APECED) in a series of 68 patients. *N. Engl. J. Med.* 322: 1829–1836. https://doi.org/10.1056/NEJM199006283222601

Anderson, M.S., E.S. Venanzi, L. Klein, Z. Chen, S.P. Berzins, S.J. Turley, H. von Boehmer, R. Bronson, A. Dierich, C. Benoist, and D. Mathis. 2002. Projection of an immunological self shadow within the thymus by the aire protein. *Science.* 298:1395–1401. https://doi.org/10.1126/science.1075958

Arbuckle, M.R., M.T. McClain, M.V. Rubertone, R.H. Scofield, G.J. Dennis, J.A. James, and J.B. Harley. 2003. Development of autoantibodies before the clinical onset of systemic lupus erythematosus. *N. Engl. J. Med.* 349: 1526–1533. https://doi.org/10.1056/NEJMoa021933

Asano, M., M. Toda, N. Sakaguchi, and S. Sakaguchi. 1996. Autoimmune disease as a consequence of developmental abnormality of a T cell subpopulation. *J. Exp. Med.* 184:387–396. https://doi.org/10.1084/jem.184.2.387

Autran, B., P. Guiet, M. Raphael, M. Grandadam, H. Agut, D. Candotti, P. Grenot, F. Puech, P. Debre, and J.Y. Cesbron. 1996. Thymocyte and thymic microenvironment alterations during a systemic HIV infection in a severe combined immunodeficient mouse model. *AIDS.* 10:717–727. https://doi.org/10.1097/00002030-199606001-00005

Barrett, S.P., B.H. Toh, F. Alderuccio, I.R. van Driel, and P.A. Gleeson. 1995. Organ-specific autoimmunity induced by adult thymectomy and cyclophosphamide-induced lymphopenia. *Eur. J. Immunol.* 25:238–244. https://doi.org/10.1002/eji.1830250139

Bautista, J.L., N.T. Cramer, C.N. Miller, J. Chavez, D.I. Berrios, L.E. Byrnes, J. Germino, V. Ntranos, J.B. Sneddon, T.D. Burt, et al. 2021. Single-cell transcriptional profiling of human thymic stroma uncovers novel cellular heterogeneity in the thymic medulla. *Nat. Commun.* 12:1096. https://doi.org/10.1038/s41467-021-21346-6

Bockerstett, K.A., L.H. Osaki, C.P. Petersen, C.W. Cai, C.F. Wong, T.M. Nguyen, E.L. Ford, D.F. Hoft, J.C. Mills, J.R. Goldenring, and R.J. DiPaolo. 2018. Interleukin-17A promotes parietal cell atrophy by inducing apoptosis. *Cell Mol. Gastroenterol. Hepatol.* 5:678–690.e1. https://doi.org/10.1016/j.jcmgh.2017.12.012

Breed, E.R., M. Watanabe, and K.A. Hogquist. 2019. Measuring thymic clonal deletion at the population level. *J. Immunol.* 202:3226–3233. https://doi.org/10.4049/jimmunol.1900191

Broccolo, F., F. Drago, G. Cassina, A. Fava, L. Fusetti, B. Matteoli, L. Ceccherini-Nelli, M.G. Sabbadini, P. Lusso, A. Parodi, and M.S. Malnati. 2013. Selective reactivation of human herpesvirus 6 in patients with autoimmune connective tissue diseases. *J. Med. Virol.* 85:1925–1934. https://doi.org/10.1002/jmv.23670

Broccolo, F., F. Drago, S. Paolino, G. Cassina, F. Gatto, L. Fusetti, B. Matteoli, E. Zaccaria, A. Parodi, P. Lusso, et al. 2009. Reactivation of human herpesvirus 6 (HHV-6) infection in patients with connective tissue diseases. *J. Clin. Virol.* 46:43–46. https://doi.org/10.1016/j.jcv.2009.05.010

Cano-Gamez, E., B. Soskic, T.I. Roumeliotis, E. So, D.J. Smyth, M. Baldrighi, D. Wille, N. Nakic, J. Esparza-Gordillo, C.G.C. Larminie, et al. 2020. Single-cell transcriptomics identifies an effectorness gradient shaping the response of $CD4^+$ T cells to cytokines. *Nat. Commun.* 11:1801. https://doi.org/10.1038/s41467-020-15543-y

Caselli, E., M. D'Accolti, I. Soffritti, M.C. Zatelli, R. Rossi, E. Degli Uberti, and D. Di Luca. 2017. HHV-6A in vitro infection of thyrocytes and T cells alters the expression of miRNA associated to autoimmune thyroiditis. *Virol. J.* 14:3. https://doi.org/10.1186/s12985-016-0672-6

Caselli, E., I. Soffritti, M. D'Accolti, D. Bortolotti, R. Rizzo, G. Sighinolfi, D. Giuggioli, and C. Ferri. 2019. HHV-6A infection and systemic sclerosis: Clues of a possible association. *Microorganisms.* 8. https://doi.org/10.3390/microorganisms8010039

Caselli, E., M.C. Zatelli, R. Rizzo, S. Benedetti, D. Martorelli, G. Trasforini, E. Cassai, E.C. degli Uberti, D. Di Luca, and R. Dolcetti. 2012. Virologic and immunologic evidence supporting an association between HHV-6 and Hashimoto's thyroiditis. *PLoS Pathog.* 8:e1002951. https://doi.org/10.1371/journal.ppat.1002951

Cheng, M., and M.S. Anderson. 2018. Thymic tolerance as a key brake on autoimmunity. *Nat. Immunol.* 19:659–664. https://doi.org/10.1038/s41590-018-0128-9

Cross, S.S., J.C. Parker, W.P. Rowe, and M.L. Robbins. 1979. Biology of mouse thymic virus, a herpesvirus of mice, and the antigenic relationship to mouse cytomegalovirus. *Infect. Immun.* 26:1186–1195. https://doi.org/10.1128/iai.26.3.1186-1195.1979

Cuende, J.I., J. Ruiz, M.P. Civeira, and J. Prieto. 1994. High prevalence of HHV-6 DNA in peripheral blood mononuclear cells of healthy individuals detected by nested-PCR. *J. Med. Virol.* 43:115–118. https://doi.org/10.1002/jmv.1890430203

D'Elios, M.M., M.P. Bergman, A. Azzurri, A. Amedei, M. Benagiano, J.J. De Pont, F. Cianchi, C.M. Vandenbroucke-Grauls, S. Romagnani, B.J. Appelmelk, and G. Del Prete. 2001. H^+,K^+-ATPase (proton pump) is the target autoantigen of Th1-type cytotoxic T cells in autoimmune gastritis. *Gastroenterology.* 120:377–386. https://doi.org/10.1053/gast.2001.21187

Denner, J., T.M. Bigley, T.L. Phan, C. Zimmermann, X. Zhou, and B.B. Kaufer. 2019. Comparative analysis of roseoloviruses in humans, pigs, mice, and other species. *Viruses.* 11:1108. https://doi.org/10.3390/v11121108

DiPaolo, R.J., D.D. Glass, K.E. Bijwaard, and E.M. Shevach. 2005. CD4+CD25+ T cells prevent the development of organ-specific autoimmune disease by inhibiting the differentiation of autoreactive effector T cells. *J. Immunol.* 175:7135–7142. https://doi.org/10.4049/jimmunol.175.11.7135

Dong, M., P. Artusa, S.A. Kelly, M. Fournier, T.A. Baldwin, J.N. Mandl, and H.J. Melichar. 2017. Alterations in the thymic selection threshold skew the self-reactivity of the TCR repertoire in neonates. *J. Immunol.* 199: 965–973. https://doi.org/10.4049/jimmunol.1602137

Douagi, I., I. Andre, J.C. Ferraz, and A. Cumano. 2000. Characterization of T cell precursor activity in the murine fetal thymus: Evidence for an input of T cell precursors between days 12 and 14 of gestation. *Eur. J. Immunol.* 30:2201–2210

Dutz, J.P., C.J. Ong, J. Marth, and H.S. Teh. 1995. Distinct differentiative stages of CD4+CD8+ thymocyte development defined by the lack of coreceptor binding in positive selection. *J. Immunol.* 154:2588–2599

Elsaesser, H.J., M. Mohtashami, I. Osokine, L.M. Snell, C.R. Cunningham, G.M. Boukhaled, D.B. McGavern, J.C. Zuniga-Pflucker, and D.G. Brooks. 2020. Chronic virus infection drives CD8 T cell-mediated thymic destruction and impaired negative selection. *Proc. Natl. Acad. Sci. USA.* 117: 5420–5429. https://doi.org/10.1073/pnas.1913776117

Faraco, G., D. Brea, L. Garcia-Bonilla, G. Wang, G. Racchumi, H. Chang, I. Buendia, M.M. Santisteban, S.G. Segarra, K. Koizumi, et al. 2018. Dietary salt promotes neurovascular and cognitive dysfunction through a gut-initiated TH17 response. *Nat. Neurosci.* 21:240–249. https://doi.org/10.1038/s41593-017-0059-z

Fujinami, R.S., and M.B. Oldstone. 1985. Amino acid homology between the encephalitogenic site of myelin basic protein and virus: Mechanism for autoimmunity. *Science.* 230:1043–1045. https://doi.org/10.1126/science.2414848

Fukuma, K., S. Sakaguchi, K. Kuribayashi, W.L. Chen, R. Morishita, K. Sekita, H. Uchino, and T. Masuda. 1988. Immunologic and clinical studies on murine experimental autoimmune gastritis induced by neonatal thymectomy. *Gastroenterology.* 94:274–283. https://doi.org/10.1016/0016-5085(88)90413-1

Garcia-Ceca, J., S. Montero-Herradon, and A.G. Zapata. 2020. Intrathymic selection and defects in the thymic epithelial cell development. *Cells.* 9: 2226. https://doi.org/10.3390/cells9102226

Gobbi, A., C.A. Stoddart, M.S. Malnati, G. Locatelli, F. Santoro, N.W. Abbey, C. Bare, V. Linquist-Stepps, M.B. Moreno, B.G. Herndier, et al. 1999. Human herpesvirus 6 (HHV-6) causes severe thymocyte depletion in SCID-hu Thy/Liv mice. *J. Exp. Med.* 189:1953–1960. https://doi.org/10.1084/jem.189.12.1953

Gruffat, H., R. Marchione, and E. Manet. 2016. Herpesvirus late gene expression: A viral-specific pre-initiation complex is key. *Front Microbiol.* 7:869. https://doi.org/10.3389/fmicb.2016.00869

Harakal, J., C. Rival, H. Qiao, and K.S. Tung. 2016. Regulatory T cells control Th2-dominant murine autoimmune gastritis. *J. Immunol.* 197:27–41. https://doi.org/10.4049/jimmunol.1502344

Hebel, K., S. Weinert, B. Kuropka, J. Knolle, B. Kosak, G. Jorch, C. Arens, E. Krause, R.C. Braun-Dullaeus, and M.C. Brunner-Weinzierl. 2014. CD4+ T cells from human neonates and infants are poised spontaneously to run a nonclassical IL-4 program. *J. Immunol.* 192:5160–5170. https://doi.org/10.4049/jimmunol.1302539

Herbin, O., A.J. Bonito, S. Jeong, E.G. Weinstein, A.H. Rahman, H. Xiong, M. Merad, and K. Alexandropoulos. 2016. Medullary thymic epithelial cells and CD8α+ dendritic cells coordinately regulate central tolerance but CD8α+ cells are dispensable for thymic regulatory T cell production. *J. Autoimmun.* 75:141–149. https://doi.org/10.1016/j.jaut.2016.08.002

Hogquist, K.A., T.A. Baldwin, and S.C. Jameson. 2005. Central tolerance: Learning self-control in the thymus. *Nat. Rev. Immunol.* 5:772–782. https://doi.org/10.1038/nri1707

Horvat, B., B.K. Berges, and P. Lusso. 2014. Recent developments in animal models for human herpesvirus 6A and 6B. *Curr. Opin. Virol.* 9:97–103. https://doi.org/10.1016/j.coviro.2014.09.012

Hsieh, C.S., Y. Zheng, Y. Liang, J.D. Fontenot, and A.Y. Rudensky. 2006. An intersection between the self-reactive regulatory and nonregulatory T cell receptor repertoires. *Nat. Immunol.* 7:401–410. https://doi.org/10.1038/ni1318

Humbert, L., M. Cornu, E. Proust-Lemoine, J. Bayry, J.L. Wemeau, M.C. Vantyghem, and B. Sendid. 2018. Chronic mucocutaneous candidiasis in autoimmune polyendocrine syndrome type 1. *Front Immunol.* 9:2570. https://doi.org/10.3389/fimmu.2018.02570

Huter, E.N., G.H. Stummvoll, R.J. DiPaolo, D.D. Glass, and E.M. Shevach. 2009. Pre-differentiated Th1 and Th17 effector T cells in autoimmune gastritis: Ag-specific regulatory T cells are more potent suppressors than polyclonal regulatory T cells. *Int. Immunopharmacol.* 9:540–545. https://doi.org/10.1016/j.intimp.2009.01.022

Jain, R., and D.H.D. Gray. 2014. Isolation of thymic epithelial cells and analysis by flow cytometry. *Curr. Protoc. Immunol.* 107:3.26.1–3.26.15. https://doi.org/10.1002/0471142735.im0326s107

Jelley-Gibbs, D.M., J.P. Dibble, S. Filipson, L. Haynes, R.A. Kemp, and S.L. Swain. 2005. Repeated stimulation of CD4 effector T cells can limit their protective function. *J. Exp. Med.* 201:1101–1112. https://doi.org/10.1084/jem.20041852

Joshi, N.S., W. Cui, A. Chandele, H.K. Lee, D.R. Urso, J. Hagman, L. Gapin, and S.M. Kaech. 2007. Inflammation directs memory precursor and short-lived effector CD8+ T cell fates via the graded expression of T-bet transcription factor. *Immunity.* 27:281–295. https://doi.org/10.1016/j.immuni.2007.07.010

Jotereau, F., F. Heuze, V. Salomon-Vie, and H. Gascan. 1987. Cell kinetics in the fetal mouse thymus: Precursor cell input, proliferation, and emigration. *J. Immunol.* 138:1026–1030

Karlsson, F.A., P. Burman, L. Loof, and S. Mardh. 1988. Major parietal cell antigen in autoimmune gastritis with pernicious anemia is the acid-producing H+,K+-adenosine triphosphatase of the stomach. *J. Clin. Invest.* 81:475–479. https://doi.org/10.1172/JCI113344

Kidzeru, E.B., A.C. Hesseling, J.A. Passmore, L. Myer, H. Gamieldien, C.T. Tchakoute, C.M. Gray, D.L. Sodora, and H.B. Jaspan. 2014. In-utero exposure to maternal HIV infection alters T-cell immune responses to vaccination in HIV-uninfected infants. *AIDS.* 28:1421–1430. https://doi.org/10.1097/QAD.0000000000000292

Kim, I., T.L. Saunders, and S.J. Morrison. 2007. Sox17 dependence distinguishes the transcriptional regulation of fetal from adult hematopoietic stem cells. *Cell.* 130:470–483. https://doi.org/10.1016/j.cell.2007.06.011

Kinnunen, T., N. Chamberlain, H. Morbach, J. Choi, S. Kim, J. Craft, L. Mayer, C. Cancrini, L. Passerini, R. Bacchetta, et al. 2013. Accumulation of peripheral autoreactive B cells in the absence of functional human regulatory T cells. *Blood.* 121:1595–1603. https://doi.org/10.1182/blood-2012-09-457465

Klocke, K., S. Sakaguchi, R. Holmdahl, and K. Wing. 2016. Induction of autoimmune disease by deletion of CTLA-4 in mice in adulthood. *Proc. Natl. Acad. Sci. USA.* 113:E2383–E2392. https://doi.org/10.1073/pnas.1603892113

Knox, K.K., D. Pietryga, D.J. Harrington, R. Franciosi, and D.R. Carrigan. 1995. Progressive immunodeficiency and fatal pneumonitis associated with human herpesvirus 6 infection in an infant. *Clin. Infect. Dis.* 20:406–413. https://doi.org/10.1093/clinids/20.2.406

Kojima, A., and R.T. Prehn. 1981. Genetic susceptibility to post-thymectomy autoimmune diseases in mice. *Immunogenetics.* 14:15–27. https://doi.org/10.1007/BF00344296

Lanari, M., I. Papa, V. Venturi, T. Lazzarotto, G. Faldella, L. Gabrielli, B. Guerra, M.P. Landini, and G.P. Salvioli. 2003. Congenital infection with human herpesvirus 6 variant B associated with neonatal seizures and poor neurological outcome. *J. Med. Virol.* 70:628–632. https://doi.org/10.1002/jmv.10441

Landegren, N., L.B. Rosen, E. Freyhult, D. Eriksson, T. Fall, G. Smith, E.M.N. Ferre, P. Brodin, D. Sharon, M. Snyder, et al. 2019. Comment on "AIRE-deficient patients harbor unique high-affinity disease-ameliorating autoantibodies". *Elife.* 8:e43578. https://doi.org/10.7554/elife.43578

Lenti, M.V., M. Rugge, E. Lahner, E. Miceli, B.H. Toh, R.M. Genta, C. De Block, C. Hershko, and A. Di Sabatino. 2020. Autoimmune gastritis. *Nat. Rev. Dis. Primers.* 6:56. https://doi.org/10.1038/s41572-020-0187-8

Lenzo, J.C., G.R. Shellam, and C.M. Lawson. 2001. Ganciclovir and cidofovir treatment of cytomegalovirus-induced myocarditis in mice. *Antimicrob. Agents Chemother.* 45:1444–1449. https://doi.org/10.1128/AAC.45.5.1444-1449.2001

Leslie, D., P. Lipsky, and A.L. Notkins. 2001. Autoantibodies as predictors of disease. *J. Clin. Invest.* 108:1417–1422. https://doi.org/10.1172/JCI14452

Linhares-Lacerda, L., C.C. Palu, M. Ribeiro-Alves, B.D. Paredes, A. Morrot, M.R. Garcia-Silva, A. Cayota, and W. Savino. 2015. Differential expression of microRNAs in thymic epithelial cells from trypanosoma cruzi acutely infected mice: Putative role in thymic atrophy. *Front Immunol.* 6:428. https://doi.org/10.3389/fimmu.2015.00428

Liston, A., D.H. Gray, S. Lesage, A.L. Fletcher, J. Wilson, K.E. Webster, H.S. Scott, R.L. Boyd, L. Peltonen, and C.C. Goodnow. 2004. Gene dosage–limiting role of Aire in thymic expression, clonal deletion, and organ-specific autoimmunity. *J. Exp. Med.* 200:1015–1026. https://doi.org/10.1084/jem.20040581

Ludwig-Portugall, I., E.E. Hamilton-Williams, C. Gottschalk, and C. Kurts. 2008. Cutting edge: CD25+ regulatory T cells prevent expansion and

induce apoptosis of B cells specific for tissue autoantigens. *J. Immunol.* 181:4447–4451. https://doi.org/10.4049/jimmunol.181.7.4447

Ma, W.T., C. Chang, M.E. Gershwin, and Z.X. Lian. 2017. Development of autoantibodies precedes clinical manifestations of autoimmune diseases: A comprehensive review. *J. Autoimmun.* 83:95–112. https://doi.org/10.1016/j.jaut.2017.07.003

Majumdar, S., M. Deobagkar-Lele, V. Adiga, A. Raghavan, N. Wadhwa, S.M. Ahmed, S.R. Rananaware, S. Chakraborty, O. Joy, and D. Nandi. 2017. Differential susceptibility and maturation of thymocyte subsets during Salmonella typhimurium infection: Insights on the roles of glucocorticoids and interferon-gamma. *Sci. Rep.* 7:40793. https://doi.org/10.1038/srep40793

Malchow, S., D.S. Leventhal, V. Lee, S. Nishi, N.D. Socci, and P.A. Savage. 2016. Aire enforces immune tolerance by directing autoreactive T cells into the regulatory T cell lineage. *Immunity*. 44:1102–1113. https://doi.org/10.1016/j.immuni.2016.02.009

Mandl, J.N., J.P. Monteiro, N. Vrisekoop, and R.N. Germain. 2013. T cell-positive selection uses self-ligand binding strength to optimize repertoire recognition of foreign antigens. *Immunity*. 38:263–274. https://doi.org/10.1016/j.immuni.2012.09.011

Marchant, A., V. Appay, M. Van Der Sande, N. Dulphy, C. Liesnard, M. Kidd, S. Kaye, O. Ojuola, G.M. Gillespie, A.L. Vargas Cuero, et al. 2003. Mature CD8$^+$ T lymphocyte response to viral infection during fetal life. *J. Clin. Invest.* 111:1747–1755. https://doi.org/10.1172/JCI17470

Marks, M., and J.L. Marks. 2016. Viral arthritis. *Clin. Med. (Lond).* 16:129–134. https://doi.org/10.7861/clinmedicine.16-2-129

McCaughtry, T.M., and K.A. Hogquist. 2008. Central tolerance: What have we learned from mice? *Semin. Immunopathol.* 30:399–409. https://doi.org/10.1007/s00281-008-0137-0

McHugh, R.S., E.M. Shevach, D.H. Margulies, and K. Natarajan. 2001a. A T cell receptor transgenic model of severe, spontaneous organ-specific autoimmunity. *Eur. J. Immunol.* 31:2094–2103.

McHugh, R.S., E.M. Shevach, and A.M. Thornton. 2001b. Control of organ-specific autoimmunity by immunoregulatory CD4$^+$CD25$^+$ T cells. *Microbes Infect.* 3:919–927. https://doi.org/10.1016/s1286-4579(01)01453-8

Melo-Lima, B.L., D.L. Esposito, B.A. da Fonseca, L.T. Figueiredo, P. Moreau, and E.A. Donadi. 2015. The attenuated live yellow fever virus 17D infects the thymus and induces thymic transcriptional modifications of immunomodulatory genes in C57BL/6 and BALB/C mice. *Autoimmune Dis.* 2015:503087. https://doi.org/10.1155/2015/503087

Mendel, I., M. de Matteis, C. Bertin, B. Delaporte, D. Maguer, H. Collandre, and C. Buffet-Janvresse. 1995. Fulminant hepatitis in neonates with human herpesvirus 6 infection. *Pediatr. Infect. Dis. J.* 14:993–997. https://doi.org/10.1097/00006454-199511000-00013

Messias, C.V., G. Loss-Morais, J.B. Carvalho, M.N. Gonzalez, D.P. Cunha, Z. Vasconcelos, L.W.P. Arge, D.A. Farias-de-Oliveira, A.L. Gerber, E.A. Portari, et al. 2020. Zika virus targets the human thymic epithelium. *Sci. Rep.* 10:1378. https://doi.org/10.1038/s41598-020-58135-y

Meyer, S., M. Woodward, C. Hertel, P. Vlaicu, Y. Haque, J. Karner, A. Macagno, S.C. Onuoha, D. Fishman, H. Peterson, et al. 2016. AIRE-deficient patients harbor unique high-affinity disease-ameliorating autoantibodies. *Cell*. 166:582–595. https://doi.org/10.1016/j.cell.2016.06.024

Mold, J.E., S. Venkatasubrahmanyam, T.D. Burt, J. Michaelsson, J.M. Rivera, S.A. Galkina, K. Weinberg, C.A. Stoddart, and J.M. McCune. 2010. Fetal and adult hematopoietic stem cells give rise to distinct T cell lineages in humans. *Science*. 330:1695–1699. https://doi.org/10.1126/science.1196509

Morse, S.S., N. Sakaguchi, and S. Sakaguchi. 1999. Virus and autoimmunity: Induction of autoimmune disease in mice by mouse T lymphotropic virus (MTLV) destroying CD4$^+$ T cells. *J. Immunol.* 162:5309–5316

Morse, S.S., and J.E. Valinsky. 1989. Mouse thymic virus (MTLV). A mammalian herpesvirus cytolytic for CD4$^+$ (L3T4$^+$) T lymphocytes. *J. Exp. Med.* 169:591–596. https://doi.org/10.1084/jem.169.2.591

Munks, M.W., K.S. Cho, A.K. Pinto, S. Sierro, P. Klenerman, and A.B. Hill. 2006. Four distinct patterns of memory CD8 T cell responses to chronic murine cytomegalovirus infection. *J. Immunol.* 177:450–458. https://doi.org/10.4049/jimmunol.177.1.450

Munz, C., J.D. Lunemann, M.T. Getts, and S.D. Miller. 2009. Antiviral immune responses: Triggers of or triggered by autoimmunity? *Nat. Rev. Immunol.* 9:246–258. https://doi.org/10.1038/nri2527

Nevins, T.E., and D.L. Dunn. 1992. Use of ganciclovir for cytomegalovirus infection. *J. Am. Soc. Nephrol.* 2:S270–S273. https://doi.org/10.1681/ASN.V212s270

Nguyen, T.L., S.S. Khurana, C.J. Bellone, B.J. Capoccia, J.E. Sagartz, R.A. Kesman Jr., J.C. Mills, and R.J. DiPaolo. 2013. Autoimmune gastritis mediated by CD4$^+$ T cells promotes the development of gastric cancer. *Cancer Res.* 73:2117–2126. https://doi.org/10.1158/0008-5472.CAN-12-3957

Nishizuka, Y., and T. Sakakura. 1969. Thymus and reproduction: Sex-linked dysgenesia of the gonad after neonatal thymectomy in mice. *Science*. 166:753–755. https://doi.org/10.1126/science.166.3906.753

Pantry, S.N., and P.G. Medveczky. 2017. Latency, integration, and reactivation of human herpesvirus-6. *Viruses*. 9. https://doi.org/10.3390/v9070194

Passos, G.A., C.A. Speck-Hernandez, A.F. Assis, and D.A. Mendes-da-Cruz. 2018. Update on Aire and thymic negative selection. *Immunology*. 153:10–20. https://doi.org/10.1111/imm.12831

Patel, S.J., and W.M. Yokoyama. 2017a. CD8$^+$ T cells prevent lethality from neonatal murine roseolovirus infection. *J. Immunol.* 199:3212–3221. https://doi.org/10.4049/jimmunol.1700982

Patel, S.J., and W.M. Yokoyama. 2017b. Reply to "Murine roseolovirus, historically known as murine thymic lymphotropic virus". *J. Virol.* 91:e00956-17. https://doi.org/10.1128/jvi.00956-17

Patel, S.J., G. Zhao, V.R. Penna, E. Park, E.J. Lauron, I.B. Harvey, W.L. Beatty, B. Plougastel-Douglas, J. Poursine-Laurent, D.H. Fremont, et al. 2017. A murine herpesvirus closely related to ubiquitous human herpesviruses causes T-cell depletion. *J. Virol.* 91:e02463-16. https://doi.org/10.1128/JVI.02463-16

Paya, C., A. Humar, E. Dominguez, K. Washburn, E. Blumberg, B. Alexander, R. Freeman, N. Heaton, and M.D. Pescovitz, and Valganciclovir Solid Organ Transplant Study Group. 2004. Efficacy and safety of valganciclovir vs. oral ganciclovir for prevention of cytomegalovirus disease in solid organ transplant recipients. *Am. J. Transpl.* 4:611–620. https://doi.org/10.1111/j.1600-6143.2004.00382.x

Perheentupa, J. 2006. Autoimmune polyendocrinopathy-candidiasis-ectodermal dystrophy. *J. Clin. Endocrinol. Metab.* 91:2843–2850. https://doi.org/10.1210/jc.2005-2611

Perniola, R. 2018. Twenty years of AIRE. *Front Immunol.* 9:98. https://doi.org/10.3389/fimmu.2018.00098

Perniola, R., A. Falorni, M.G. Clemente, F. Forini, E. Accogli, and G. Lobreglio. 2000. Organ-specific and non-organ-specific autoantibodies in children and young adults with autoimmune polyendocrinopathy-candidiasis-ectodermal dystrophy (APECED). *Eur. J. Endocrinol.* 143:497–503. https://doi.org/10.1530/eje.0.1430497

Perry, J.S.A., C.J. Lio, A.L. Kau, K. Nutsch, Z. Yang, J.I. Gordon, K.M. Murphy, and C.S. Hsieh. 2014. Distinct contributions of Aire and antigen-presenting-cell subsets to the generation of self-tolerance in the thymus. *Immunity*. 41:414–426. https://doi.org/10.1016/j.immuni.2014.08.007

Plumlee, C.R., B.S. Sheridan, B.B. Cicek, and L. Lefrancois. 2013. Environmental cues dictate the fate of individual CD8$^+$ T cells responding to infection. *Immunity*. 39:347–356. https://doi.org/10.1016/j.immuni.2013.07.014

Price, P., S.D. Olver, A.E. Gibbons, H.K. Teo, and G.R. Shellam. 1993. Characterization of thymic involution induced by murine cytomegalovirus infection. *Immunol. Cell Biol.* 71(Pt 3):155–165. https://doi.org/10.1038/icb.1993.18

Ribot, J., G. Enault, S. Pilipenko, A. Huchenq, M. Calise, D. Hudrisier, P. Romagnoli, and J.P. van Meerwijk. 2007. Shaping of the autoreactive regulatory T cell repertoire by thymic cortical positive selection. *J. Immunol.* 179:6741–6748. https://doi.org/10.4049/jimmunol.179.10.6741

Rogers, A.B., N.S. Taylor, M.T. Whary, E.D. Stefanich, T.C. Wang, and J.G. Fox. 2005. Helicobacter pylori but not high salt induces gastric intraepithelial neoplasia in B6129 mice. *Cancer Res.* 65:10709–10715. https://doi.org/10.1158/0008-5472.can-05-1846

Rolot, M., A.M. Dougall, A. Chetty, J. Javaux, T. Chen, X. Xiao, B. Machiels, M.E. Selkirk, R.M. Maizels, C. Hokke, et al. 2018. Helminth-induced IL-4 expands bystander memory CD8$^+$ T cells for early control of viral infection. *Nat. Commun.* 9:4516. https://doi.org/10.1038/s41467-018-06978-5

Rowe, W.P., and W.I. Capps. 1961. A new mouse virus causing necrosis of the thymus in newborn mice. *J. Exp. Med.* 113:831–844. https://doi.org/10.1084/jem.113.5.831

Ruan, Q.G., K. Tung, D. Eisenman, Y. Setiady, S. Eckenrode, B. Yi, S. Purohit, W.P. Zheng, Y. Zhang, L. Peltonen, and J.X. She. 2007. The autoimmune regulator directly controls the expression of genes critical for thymic epithelial function. *J. Immunol.* 178:7173–7180. https://doi.org/10.4049/jimmunol.178.11.7173

Rudd, B.D. 2020. Neonatal T cells: A reinterpretation. *Annu. Rev. Immunol.* 38:229–247. https://doi.org/10.1146/annurev-immunol-091319-083608

Saito, T., S. Suenaga, M. Fujii, Y. Kushida, Y. Kawauchi, K. Suzuki, M. Touma, and M. Hosono. 2016. Induction of autoimmune gastritis by neonatal thymectomy requires autoantibodies and is prevented by anti-FcγR antibodies. *Cell Immunol.* 300:1–8. https://doi.org/10.1016/j.cellimm.2015.10.004

Sakaguchi, S., K. Fukuma, K. Kuribayashi, and T. Masuda. 1985. Organ-specific autoimmune diseases induced in mice by elimination of T cell subset. I. Evidence for the active participation of T cells in natural self-tolerance; deficit of a T cell subset as a possible cause of autoimmune disease. *J. Exp. Med.* 161:72–87. https://doi.org/10.1084/jem.161.1.72

Sakaguchi, S., N. Sakaguchi, M. Asano, M. Itoh, and M. Toda. 1995. Immunologic self-tolerance maintained by activated T cells expressing IL-2 receptor alpha-chains (CD25). Breakdown of a single mechanism of self-tolerance causes various autoimmune diseases. *J. Immunol.* 155:1151–1164.

Santos, C.A. 2016. Cytomegalovirus and other beta-herpesviruses. *Semin. Nephrol.* 36:351–361. https://doi.org/10.1016/j.semnephrol.2016.05.012

Savino, W. 2006. The thymus is a common target organ in infectious diseases. *PLoS Pathog.* 2:e62. https://doi.org/10.1371/journal.ppat.0020062

Scarff, K.J., J.M. Pettitt, I.R. Van Driel, P.A. Gleeson, and B.H. Toh. 1997. Immunization with gastric H^+/K^+-ATPase induces a reversible autoimmune gastritis. *Immunology*. 92:91–98. https://doi.org/10.1046/j.1365-2567.1997.00302.x

Sell, S., M. Dietz, A. Schneider, R. Holtappels, M. Mach, and T.H. Winkler. 2015. Control of murine cytomegalovirus infection by gammadelta T cells. *PLoS Pathog.* 11:e1004481. https://doi.org/10.1371/journal.ppat.1004481

Sng, J., B. Ayoglu, J.W. Chen, J.N. Schickel, E.M.N. Ferre, S. Glauzy, N. Romberg, M. Hoenig, C. Cunningham-Rundles, P.J. Utz, et al. 2019. AIRE expression controls the peripheral selection of autoreactive B cells. *Sci. Immunol.* 4:eaav6778. https://doi.org/10.1126/sciimmunol.aav6778

Stummvoll, G.H., R.J. DiPaolo, E.N. Huter, T.S. Davidson, D. Glass, J.M. Ward, and E.M. Shevach. 2008. Th1, Th2, and Th17 effector T cell-induced autoimmune gastritis differs in pathological pattern and in susceptibility to suppression by regulatory T cells. *J. Immunol.* 181:1908–1916. https://doi.org/10.4049/jimmunol.181.3.1908

Suri-Payer, E., A.Z. Amar, R. McHugh, K. Natarajan, D.H. Margulies, and E.M. Shevach. 1999. Post-thymectomy autoimmune gastritis: Fine specificity and pathogenicity of anti-H/K ATPase-reactive T cells. *Eur. J. Immunol.* 29:669–677. https://doi.org/10.1002/(SICI)1521-4141(199902)29:02<669::AID-IMMU669>3.0.CO;2-J

Suri-Payer, E., A.Z. Amar, A.M. Thornton, and E.M. Shevach. 1998. $CD4^+CD25^+$ T cells inhibit both the induction and effector function of autoreactive T cells and represent a unique lineage of immunoregulatory cells. *J. Immunol.* 160:1212–1218.

Suri-Payer, E., P.J. Kehn, A.W. Cheever, and E.M. Shevach. 1996. Pathogenesis of post-thymectomy autoimmune gastritis. Identification of anti-H/K adenosine triphosphatase-reactive T cells. *J. Immunol.* 157:1799–1805.

Taguchi, O., and Y. Nishizuka. 1987. Self tolerance and localized autoimmunity. Mouse models of autoimmune disease that suggest tissue-specific suppressor T cells are involved in self tolerance. *J. Exp. Med.* 165:146–156. https://doi.org/10.1084/jem.165.1.146

Takaba, H., and H. Takayanagi. 2017. The mechanisms of T cell selection in the thymus. *Trends Immunol.* 38:805–816. https://doi.org/10.1016/j.it.2017.07.010

Tanner, A., S.A. Carlson, M. Nukui, E.A. Murphy, and B.K. Berges. 2013. Human herpesvirus 6A infection and immunopathogenesis in humanized $Rag2^{-/-}$ $\gamma c^{-/-}$ mice. *J. Virol.* 87:12020–12028. https://doi.org/10.1128/JVI.01556-13

Tu, E., D.K. Ang, S.A. Bellingham, T.V. Hogan, M.W. Teng, M.J. Smyth, A.F. Hill, and I.R. van Driel. 2012. Both IFN-gamma and IL-17 are required for the development of severe autoimmune gastritis. *Eur. J. Immunol.* 42:2574–2583. https://doi.org/10.1002/eji.201142341

Valentin, H., O. Azocar, B. Horvat, R. Williems, R. Garrone, A. Evlashev, M.L. Toribio, and C. Rabourdin-Combe. 1999. Measles virus infection induces terminal differentiation of human thymic epithelial cells. *J. Virol.* 73:2212–2221. https://doi.org/10.1128/JVI.73.3.2212-2221.1999

van Faassen, H., M. Saldanha, D. Gilbertson, R. Dudani, L. Krishnan, and S. Sad. 2005. Reducing the stimulation of $CD8^+$ T cells during infection with intracellular bacteria promotes differentiation primarily into a central (CD62LhighCD44high) subset. *J. Immunol.* 174:5341–5350. https://doi.org/10.4049/jimmunol.174.9.5341

Velardi, E., J.J. Tsai, and M.R.M. van den Brink. 2020. T cell regeneration after immunological injury. *Nat. Rev. Immunol.* 21:277–291. https://doi.org/10.1038/s41577-020-00457-z

Wang, B., Y. Saito, M. Nishimura, Z. Ren, L.H. Tjan, A. Refaat, R. Iida-Norita, R. Tsukamoto, M. Komatsu, T. Itoh, et al. 2020. An animal model that mimics human herpesvirus 6B pathogenesis. *J. Virol.* 94:e01851-19. https://doi.org/10.1128/JVI.01851-19

Wang, J., E.M. Wissink, N.B. Watson, N.L. Smith, A. Grimson, and B.D. Rudd. 2016. Fetal and adult progenitors give rise to unique populations of $CD8^+$ T cells. *Blood*. 128:3073–3082. https://doi.org/10.1182/blood-2016-06-725366

Wardemann, H., S. Yurasov, A. Schaefer, J.W. Young, E. Meffre, and M.C. Nussenzweig. 2003. Predominant autoantibody production by early human B cell precursors. *Science*. 301:1374–1377. https://doi.org/10.1126/science.1086907

Winter, S., A. Rehm, K. Wichner, T. Scheel, A. Batra, B. Siegmund, C. Berek, M. Lipp, and U.E. Hopken. 2011. Manifestation of spontaneous and early autoimmune gastritis in CCR7-deficient mice. *Am. J. Pathol.* 179:754–765. https://doi.org/10.1016/j.ajpath.2011.04.012

Yamada, A., A. Ushio, R. Arakaki, T. Tsunematsu, Y. Kudo, Y. Hayashi, and N. Ishimaru. 2015. Impaired expansion of regulatory T cells in a neonatal thymectomy-induced autoimmune mouse model. *Am. J. Pathol.* 185:2886–2897. https://doi.org/10.1016/j.ajpath.2015.07.007

Yang, S., N. Fujikado, D. Kolodin, C. Benoist, and D. Mathis. 2015. Immune tolerance. Regulatory T cells generated early in life play a distinct role in maintaining self-tolerance. *Science*. 348:589–594. https://doi.org/10.1126/science.aaa7017

Yoshikawa, T., K. Suzuki, K. Umemura, S. Akimoto, F. Miyake, C. Usui, A. Fujita, S. Suga, and Y. Asano. 2004. Atypical clinical features of a human herpesvirus-6 infection in a neonate. *J. Med. Virol.* 74:463–466. https://doi.org/10.1002/jmv.20199

Zens, K.D., J.K. Chen, R.S. Guyer, F.L. Wu, F. Cvetkovski, M. Miron, and D.L. Farber. 2017. Reduced generation of lung tissue-resident memory T cells during infancy. *J. Exp. Med.* 214:2915–2932. https://doi.org/10.1084/jem.20170521

Zerr, D.M., A.S. Meier, S.S. Selke, L.M. Frenkel, M.L. Huang, A. Wald, M.P. Rhoads, L. Nguy, R. Bornemann, R.A. Morrow, and L. Corey. 2005. A population-based study of primary human herpesvirus 6 infection. *N. Engl. J. Med.* 352:768–776. https://doi.org/10.1056/NEJMoa042207

Zhao, B., L. Chang, H. Fu, G. Sun, and W. Yang. 2018. The role of autoimmune regulator (AIRE) in peripheral tolerance. *J. Immunol. Res.* 2018:3930750. https://doi.org/10.1155/2018/3930750

Zhao, D.M., A.M. Thornton, R.J. DiPaolo, and E.M. Shevach. 2006. Activated $CD4^+CD25^+$ T cells selectively kill B lymphocytes. *Blood*. 107:3925–3932. https://doi.org/10.1182/blood-2005-11-4502

Zhao, M., J. Qin, H. Yin, Y. Tan, W. Liao, Q. Liu, S. Luo, M. He, G. Liang, Y. Shi, et al. 2016. Distinct epigenomes in $CD4^+$ T cells of newborns, middle-ages and centenarians. *Sci. Rep.* 6:38411. https://doi.org/10.1038/srep38411

JEM

Supplemental material

A

Gastritis Scoring Criterion	Score				
	0	1	2	3	4
Inflammation	No inflammatory infiltrate	Patchy infiltration of mixed leukocytes in mucosa and/or submucosa	Multifocal-to-coalescing leukocyte infiltration not extending below submucosa	Marked increase in leukocytes with lymphoid follicles ± extension into tunica muscularis	Effacing transmural inflammation
Mucous metaplasia *	None	Rare small foci in corpus	Moderately large foci affecting <1/3 of mucosa	Large foci affecting 1/3-2/3 of mucosa	Foamy change affecting >2/3 of mucosa
Oxyntic gland atrophy	Normal	<50% chief cell loss, <25% parietal cell loss	~75% chief cell loss, ~50% parietal cell loss	~75% parietal cell loss, no chief cells	>75% parietal cell loss, no chief cells

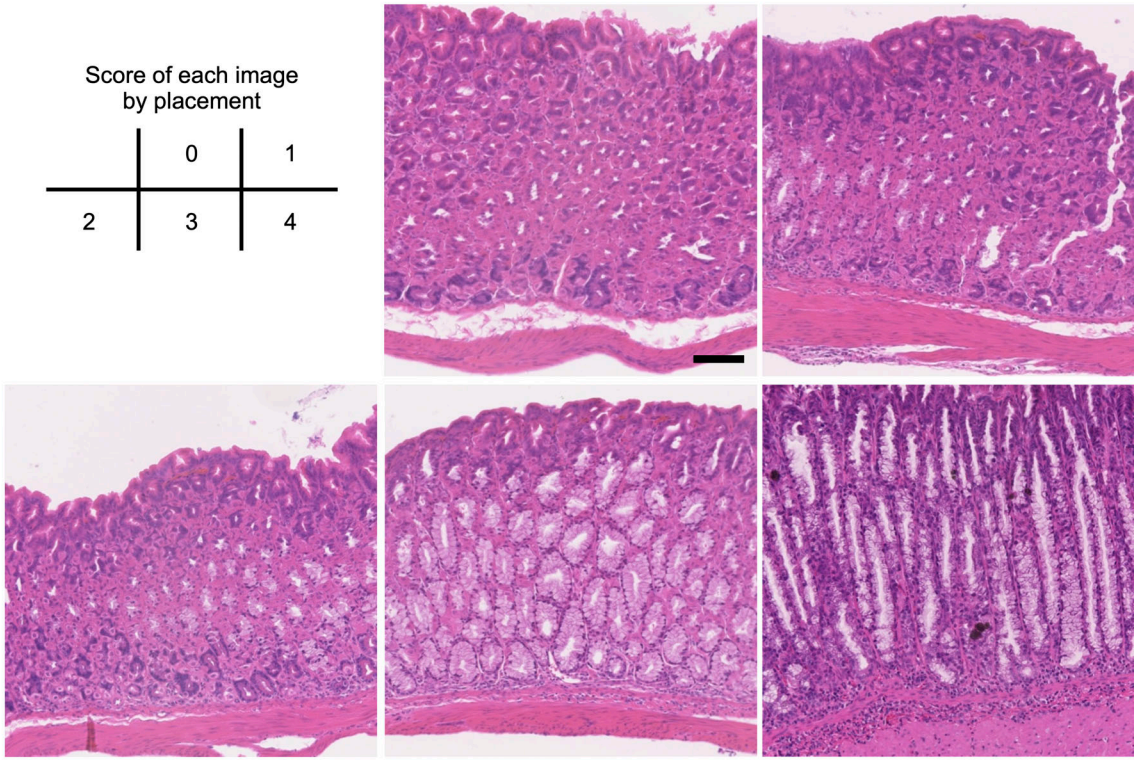

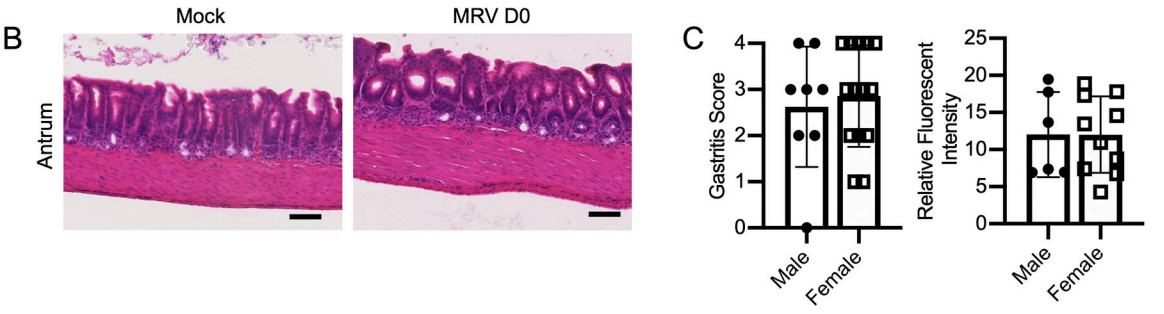

Figure S1. **Gastritis scoring criteria, evaluation of antrum inflammation, and comparison of AIG in different sexes. (A)** Gastritis scoring criteria with representative images of each score. **(B)** Representative H&E staining of the antrum of 12-wk-old mock- or D0 MRV-infected mice (scale bar = 100 µm, same scale for all images). **(C)** Gastritis scoring and relative autoantibody fluorescence intensity level of male (n = 8) and female mice (n = 10) from three independent experiments.

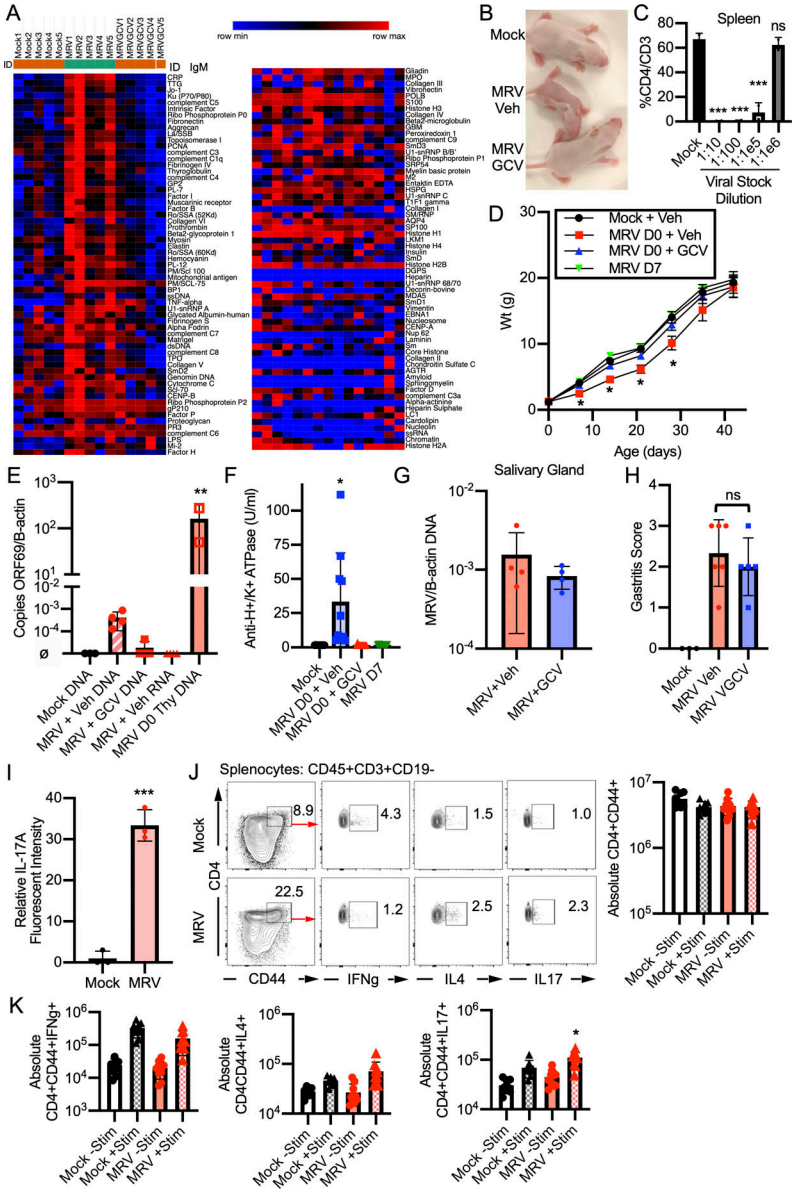

Figure S2. **Impact of neonatal MRV infection and GCV treatment on IgM autoantibodies, disease, and Th cell differentiation. (A)** BALB/c mice were mock or MRV infected on D0 and treated with vehicle control (Mock and MRV) or GCV for 7 d (MRVGCV). At 12 wk, sera were collected and evaluated using an autoantigen microarray for presence of IgM autoantibody. Each column represents serum from one mouse from the indicated experimental condition. The scale represents row minimum and maximum based on autoantibody levels. BALB/c mice were mock or MRV infected on D0 and treated with vehicle control or GCV for 7 d as in Fig. 3. **(B)** Photograph of mock infection or MRV D0 infection treated with vehicle (MRV veh) or GCV (MRV GCV) at 7 dpi. **(C)** Viral stock was serially diluted as indicated, and BALB/c mice were i.p. infected on D0 with the indicated viral stock dilution. On 7 dpi, spleens from mock or MRV viral stock infections were dissected and analyzed by flow cytometry. Statistical significance was calculated used one-way ANOVA; asterisks represent statistical significance compared with mock. **(D)** Mice were weighed every 7 d for 6 wk (mock + veh, $n = 8$; MRV D0 + Veh, $n = 10$; MRV D0 + GCV, $n = 10$; MRV D7, $n = 8$; from two independent experiments). **(E)** Mice were mock or MRV infected and treated with vehicle control or GCV for 7 d. At 7 dpi, mice were euthanized, and stomachs or thymus were evaluated for levels of ORF69 per B-actin DNA copies by qPCR or *ORF69* RNA expression using quantitative RT-PCR (stomach DNA: mock, $n = 3$; MRV + Veh, $n = 4$; MRV + GCV, $n = 4$; MRV + Veh RNA, $n = 4$; thymus: MRV D0 Thy DNA, $n = 3$; from two experiments). **(F)** Anti-H^+/K^+ ATPase ELISA was performed on sera collected from mice at 12 wk of life, and statistical significance was determined using one-way ANOVA. **(G)** Mice were infected on D0 and treated with vehicle control (MRV + Veh) or GCV (MRV + GCV) for the first 7 d of life, and then salivary glands were harvested at 12 wpi and evaluated for MRV DNA copies per β-actin (B-actin) DNA copies (MRV + Veh, $n = 4$; MRV + GCV, $n = 4$; from two independent experiments). **(H)** Mice were mock or MRV infected on D0 and treated with vehicle control chow or VGCV chow starting at 8 wk. At 12 wk, stomachs were dissected, H&E stained, and scored for gastritis (mock, $n = 3$; MRV Veh, $n = 6$; MRV VGCV, $n = 5$; combined from two independent infections). **(I)** Gastric mucosa from 12-wk-old mock or MRV D0-infected mice was sectioned and stained with DAPI (blue) and anti–IL-17A and imaged by immunofluorescence as in Fig. 5. Relative IL-17A fluorescence intensity was scored from one representative image from three different mice for each condition. **(J and K)** At 12 wk after neonatal infection, spleens were harvested, stimulated (Stim) with phorbol myristate acetate and ionomycin in vitro, evaluated by flow cytometry for cytokine expression compared to unstimulated splenocytes, and quantified as absolute number of $CD4^+CD44^+$ cells or $CD4^+CD44^+$ cells positive for cytokine expression, with representative flow plots shown. Statistical significance was calculated using multiple one-way ANOVA (C–F and J), Student's *t* test (G and I), or nonparametric Kruskal–Wallis one-way ANOVA (H). *, $P < 0.05$; **, $P < 0.01$; ***, $P < 0.001$.

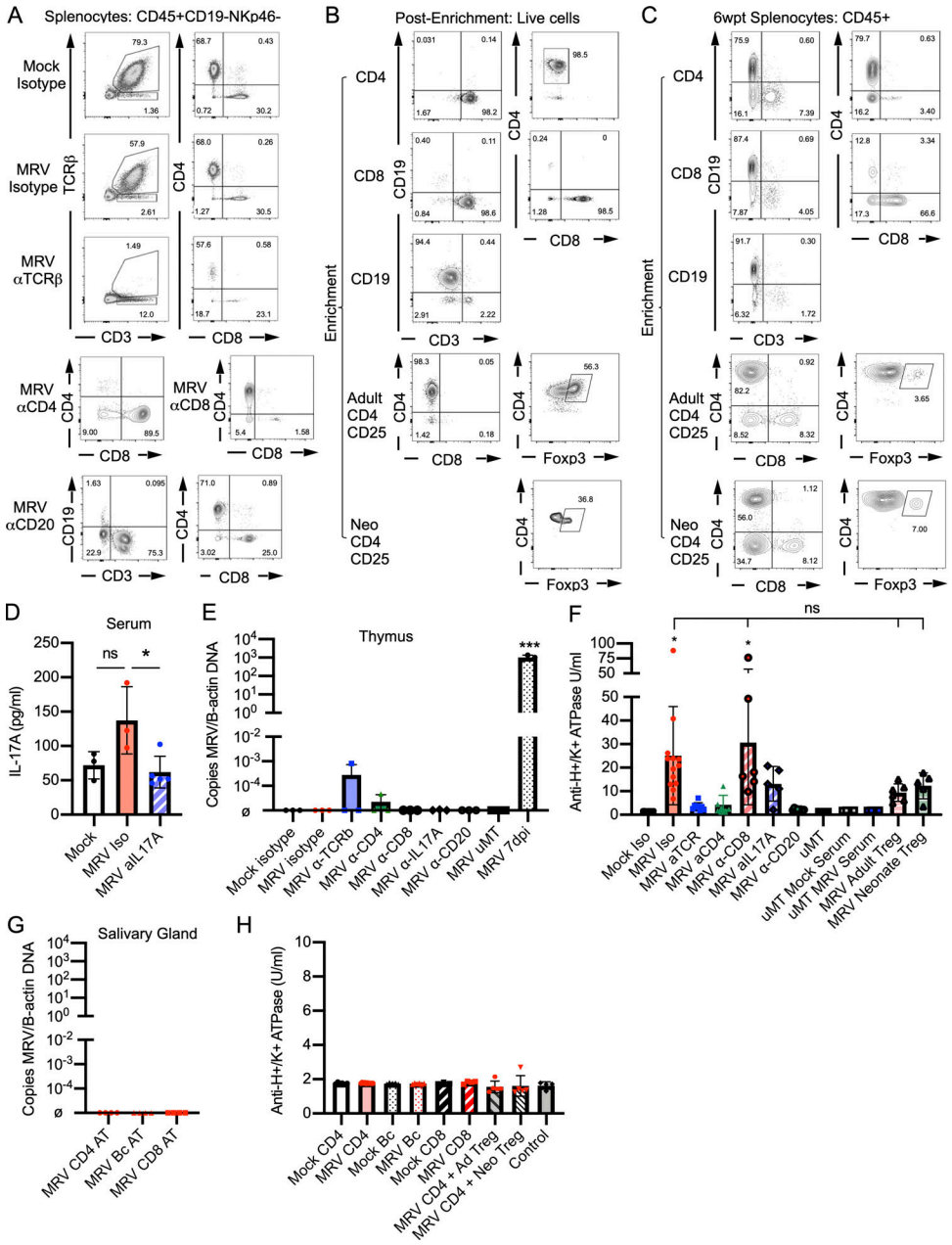

Figure S3. **CD4⁺ T cells are necessary and sufficient for MRV-mediated AIG.** BALB/c or μMT mice were mock or MRV infected on D0. MRV-infected BALB/c mice were treated with isotype control, anti-TCRβ, anti-CD4, or anti-CD8 starting at 6 wk or anti-IL17A starting at 8 wk. μMT mice were infected with MRV on D0. At 11 wk, μMT mice were either untreated or i.p. injected with serum from 12-wk-old mock- or D0 MRV-infected mice. For adoptive transfer, 8-wk-old D0 MRV-infected mice were given 1 × 10^6 adult Tregs (MRV Adult Treg) or 1.5 × 10^5 neonatal Tregs (MRV Neonate Treg) from uninfected 12- or 1-wk-old mice. **(A and D)** At 12 wk, splenocytes were evaluated using flow cytometry, with representative flow plots shown (A) or for IL-17A serum levels after treatment with anti–IL-17A using an IL-17A ELISA (mock, *n* = 3; MRV Iso, *n* = 3; MRV aIL17A, *n* = 5; at least one replicate from two experiments; D). **(B and C)** BALB/c mice were mock or MRV infected on D0. At 12 wk, splenocytes and stomach-draining lymph node lymphocytes were enriched for total CD4⁺ T cells (CD4), CD19 B cells (Bc), CD8⁺ T cells (CD8), CD4⁺ conventional T cells, and Tregs (Adult CD4CD25) or from 1-wk-old neonatal splenocytes and stomach draining lymph node lymphocyte CD4⁺ conventional T cells and Tregs (Neo CD4CD25). The enriched samples were analyzed by flow cytometry, with representative flow plots shown. 1 × 10^7 enriched total CD4⁺ T cells (CD4), CD19 B cells (Bc), CD8⁺ T cells, or 1 × 10^7 CD4⁺ conventional T cells combined with either 1 × 10^6 adult Tregs or 1.5 × 10^5 neonatal Tregs were adoptively transferred to 6–8-wk-old athymic nude mice via i.v. injection; at 6 wk after transfer (wpt), spleens were harvested and evaluated using flow cytometry (C). **(E)** MRV DNA levels in the thymus for mice from Fig. 5 A were measured by qPCR for ORF69 relative to B-actin, with DNA from thymus of D0 MRV-infected mice, harvested on 7 dpi (MRV 7 dpi) as a control (*n* = 3 for all conditions, at least one replicate from two to three independent experiments). **(F)** Anti-H⁺/K⁺ ATPase ELISA was performed from sera collected from mice at 12 wk of life as in Fig. 6 C, and statistical significance was determined using one-way ANOVA with asterisks representing statistical significance compared to Mock Iso. **(G)** MRV DNA from nude mice receiving adoptive transfer as in Fig. 6 D was measured by copies of ORF69 transcripts relative to B-actin in salivary glands 6 wk after transfer (*n* = 3 with at least one replicate from two to three independent experiments); ø indicates below level of detection. **(H)** Anti-H⁺/K⁺ ATPase ELISA was performed from sera collected from mice at 6 wk after transfer as in Fig. 6 D. Control nude mice did not receive adoptive transfer. For C and D, there were no statistically significant differences found using one-way ANOVA. *, P < 0.05; ***, P < 0.001.

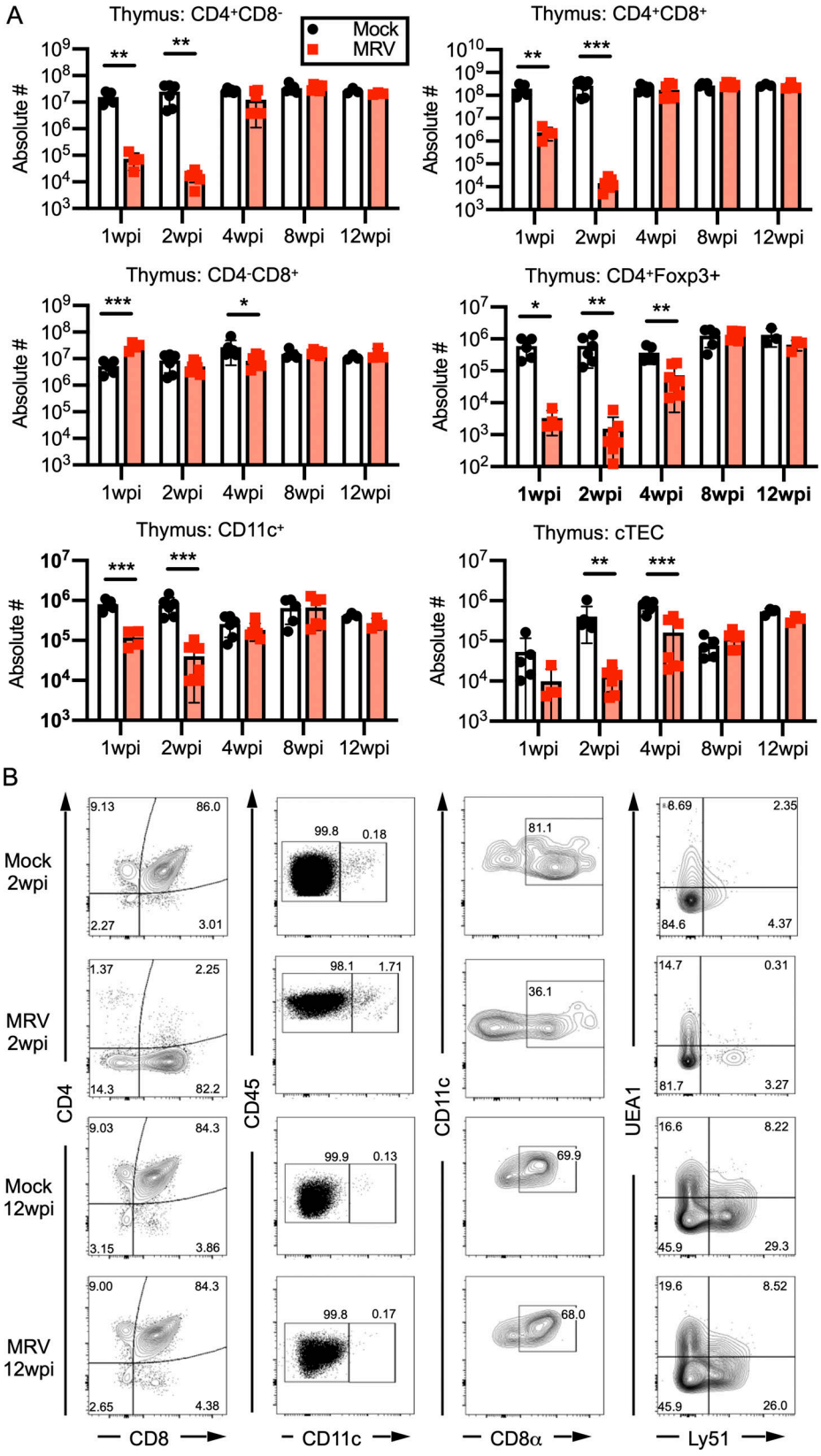

Figure S4. **Neonatal MRV infection results in transient decreases in CD4 SP and DP T cells, Tregs, cortical thymic epithelial cells, and CD11C⁺ cells. (A and B)** BALB/c mice were mock or MRV infected on D0 and harvested at various time points for flow cytometry of the thymus (as in Fig. 8) shown as absolute number (#) of cells per thymus (A), with representative flow plots shown in B. **(B)** Flow plots of thymic cell populations at 2 and 12 wpi of mice either mock or D0 MRV infected. Statistical significance for A was evaluated used multiple comparison Student's *t* test for flow cytometry. *, P < 0.05; **, P < 0.01; ***, P < 0.001.

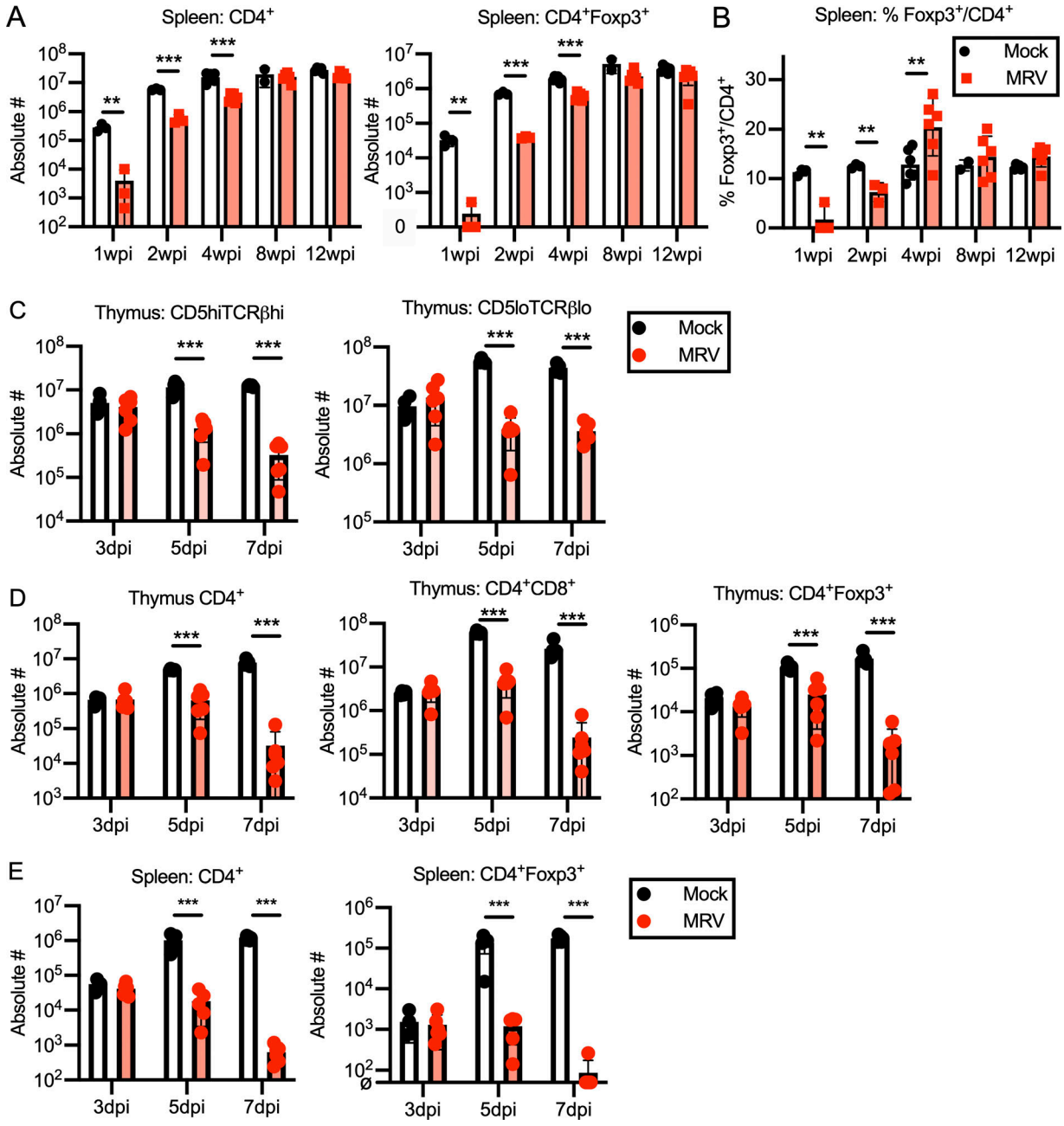

Figure S5. **Neonatal MRV infection results in transiently decreased CD4⁺ T cells in the periphery. (A and B)** BALB/c mice were mock or MRV infected on D0 and harvested at various time points for flow cytometry of the spleen, shown as absolute number (#) of cells per spleen (A), or percentage Foxp3⁺ cells per total CD4⁺ cells (B). *n* = 3–6 for each time point from two independent infections. Statistical significance was evaluated used multiple comparison Student's *t* test for flow cytometry. **(C–E)** D0 mock- or MRV-infected thymus from mice 3, 5, or 7 dpi were evaluated by flow cytometry. CD19⁻NKp46⁻TCRγδ⁻CD25⁻ (Lin⁻) cells were gated on CD5, and TCRβ surface expression and absolute number (#) were evaluated for $CD5^{hi}TCR\beta^{hi}$ or $CD5^{lo}TCR\beta^{lo}$ (C) and CD4 SP (CD4⁺), DP (CD4⁺CD8⁺), or CD4⁺Foxp3⁺ (D). Splenocytes were evaluated at the designated time points and evaluated for absolute number (#) of total CD4⁺ cells or CD4⁺Foxp3⁺ Tregs (E). *n* = 6 for all except mock 3 dpi (*n* = 4), each from two to three separate infections. Statistical significance was calculated using multiple comparison Student's *t* test. **, P < 0.01; ***, P < 0.001.